TOPICAL REPORT: SIMULATION MODEL ANALYSIS OF THE MOST PROMISING GEOLOGIC SEQUESTRATION FORMATION CANDIDATES IN THE ROCKY MOUNTAIN REGION, USA, WITH FOCUS ON UNCERTAINTY ASSESSMENT

Type of Report: Topical Report

Reporting Period Start Date: December 8, 2009
Reporting Period End Date: September 30, 2013

Principal Authors of this report:
Si-Yong Lee, University of Utah
Wade Zaluski, Schlumberger Carbon Services
Robert Will, Schlumberger Carbon Services
Chris Eisinger, Colorado Geological Survey
Vince Matthews, Colorado Geological Survey
Brian McPherson, University of Utah

Date Report was Issued: December 31, 2013

DOE Award Number DE-FE0001812

Submitting Organization:
University of Utah
Department of Civil and Environmental Engineering
Salt Lake City, Utah 84112 USA

DISCLAIMER

Abstract

The purpose of this report is to report results of reservoir model simulation analyses for forecasting subsurface CO_2 storage capacity estimation for the most promising formations in the Rocky Mountain region of the USA. A particular emphasis of this project was to assess uncertainty of the simulation-based forecasts. Results illustrate how local-scale data, including well information, number of wells, and location of wells, affect storage capacity estimates and what degree of well density (number of wells over a fixed area) may be required to estimate capacity within a specified degree of confidence. A major outcome of this work was development of a new workflow of simulation analysis, accommodating the addition of "random pseudo wells" to represent virtual characterization wells.

Table of Contents

Executive Summary

Using reservoir model simulation analysis, we evaluated the uncertainty in subsurface CO_2 storage capacity estimation for the most promising formations in the Rocky Mountain region of the USA. We also demonstrated how local data (e.g., well data, number of wells, and location of wells) affect storage capacity estimates and what degree of well density (number of wells) may be required to estimate capacity within a specified degree of confidence. To do this, we developed a new workflow of simulation analysis, accommodating the addition of "random pseudo wells" to represent the virtual characterization wells.

We focused on three potential storage formations (Weber, Entrada, and Dakota sandstone formations) within Sand Wash Basin. Geocellular model was constructed based on the stratigraphic formation top picks, well information, and well log images available from the project site. Using the sample variogram results, porosity values to each cell were assigned by the Sequential Gaussian Simulation (SGS) for each Dakota, Entrada and Weber Formation. It was assumed that the 3-D geocellular model (porosity) within the basin boundary serves as a true or best estimate of real geology.

A new workflow was developed focusing on randomly placing "pseudo-wells" in the Sand Wash Basin geocellular model. Each random pseudo-well was assumed to provide new well data and additional geologic information. We evaluated how the degrees of data density (well density) represented by the pseudo-wells affects the capacity estimates of target formations. The estimated pore volume was considered as a proxy to the capacity estimate in this work.

As each pseudo-well was placed, porosity and formation thickness information within each well was extracted from the geocellular model. Starting from a first randomly sampled point, we sequentially added a new random pseudo-well into the previous well(s) up to 25 total wells and calculated the estimated pore volume at each step to see how the new information affects the capacity estimates. Average porosity value and thickness of a target formation were determined from each pseudo-well and assigned uniformly to the subarea corresponding to the pseudo-well. The estimated pore volume of a subarea was simply computed by the product of average porosity value, thickness, and size of the subarea. The boundary of each subarea was determined by the closest distance from each pseudo-well. Total estimated pore volume of the basin is the sum of each subarea's estimated pore volume. We repeated the same process for a total of 25 cases with a different starting pseudo-well location for statistical analysis.

Relative differences of the capacity estimates from the true value of geocellular model were computed for Dakota, Entrada, and Weber formation, respectively for 25 cases. Our findings can be summarized as follows:

- Difference between the estimated pore volume and true value is generally decreasing with the addition of new data (pseudo-wells).
- Pore volume estimation for the Dakota shows better fit especially with less number of pseudo-wells compared to Entrada and Weber formation.
- Dakota formation has relatively less spatial variation in the porosity and thickness.

- Targeting ±30% relative difference as a tolerable error range, we would need at least 5 and 9 characterization wells for the Dakota and 9 wells for Entrada and Weber formations, respectively.
- The range/distribution of relative difference value for the small number of wells is significantly larger for the Entrada and Weber formation compared to the Dakota.
- Appropriate density of characterization data/well is dependent on the geologic formations even within the same basin.

As our relative difference measurement shows the deviation from the true value, we also analyzed which factor is more significant in terms of pore volume estimation. Since the estimated pore volume of a subarea is computed with the single porosity and thickness value given by the corresponding pseudo-well, the difference will increase if there is a large spatial variation in the porosity and thickness within a subarea. We calculated volume-weighted average dip angle of each target formation. Being consistent with our relative difference measurements, the volume-weighted dip angle for the Dakota is the smallest (4.95 degrees) among three target formations. Entrada and Weber are characterized by higher volume-weighted dip angle of 11.32 and 9.49 degrees, respectively. That is, a formation with a large dip angle is likely to have more uncertainty and greater error in the capacity estimation with the limited characterization data. However, unlike the volume-weighted average dip angle, the degree of heterogeneity in the porosity was not consistent with our relative difference results.

Narrative

1. Introduction

Geologic storage of CO_2 in deep geologic formations is considered one of the potential options for mitigating CO_2 emissions contributing to climate change [*IPCC*, 2007]. However, CO_2 storage potential should be understood beforehand to properly determine and deploy the carbon capture and storage (CCS) technologies. To identify and evaluate the suitable storage sites and their capacity estimates initially involves site characterization which is based on the available existing data.

During the characterization activity, potential of a site/reservoir for CO_2 storage is generally examined by three criteria: capacity, injectivity, and seal integrity.

- Capacity defines how much CO_2 can be stored within a target formation in terms of available pore space (e.g., porosity, thickness, and areal extent) for the storage.

- -Injectivity is dependent on permeability, fracture pressure; geometry and connectivity, and CO_2-water-rock interactions, which determines the relative mobility of CO_2 within the pore space.

- -Caprock or seal integrity is the ability to contain CO_2 within the injection zone determined by seal extent, fault stability and maximum sustainable fluid pressure.

Due to the lack economic interest, CCS target formations (especially saline aquifer) typically have relatively low well penetration compared to hydrocarbon production reservoirs. Therefore, the available subsurface data sets within the potential CCS target formations are often sparse and suffer from a relatively higher level of uncertainty. In order to understand this

uncertainty, we focused on the uncertainty in the storage capacity estimation and demonstrated how the local data (e.g., well data, number of wells, and location of wells) affect the storage capacity estimates and what the degree of well density (number of wells) is required to appropriately estimate the capacity within a specified degree of confidence. In other words, this study is not intended to provide specifics as to the true storage capacity of a reservoir/basin, but is intended to provide an understanding how much information is required in the characterization process to adequately estimate the storage capacity in practice. To do this, we developed a new workflow accommodating the addition of random pseudo wells to represent the virtual characterization wells.

2. Study Area

Our study focuses on the Sand Wash Basin which is a sub-basin of the Greater Green River Basin separated by east-west anticlinal ridge (Cherokee Arch) along the Colorado/Wyoming border. Three potential storage formations were identified for CO_2 injection, with general characteristics listed in Table 1. The Weber, Entrada, and Dakota sandstone formations are deep saline aquifer targets. The Weber and Entrada formations consist of mostly eolian deposits and the Dakota is comprised of fluvial and marginal marine deposits.

Within the Sand Wash Basin, regional dips are typically between 5 and 13 degrees north into the basin. South of the proposed injection site, dips become steeper (~10 to 15 degrees or more). Superimposed on the regional north dip, asymmetrical anticlines plunge northwest into the basin. The southwestern limbs of these anticlines are typically steeply dipping forced folds and possibly faulted. Structural closure is created by the Axial Basin Uplift to the south. Additionally, thinning of the Entrada Formation to the southeast creates a stratigraphic trapping

mechanism in this layer. For the Dakota and Weber Formations, migration up dip will be limited by porosity and permeability barriers. Locally, there are no known faults to act as significant leakage pathways.

Table 1. Lithology and depositional environment of the identified target formations.

Target Formation	Age	Lithology	Depositional Environment
Weber	Mid-Pennsylvanian & Lower Permian	Fine to medium-grained, siliceous sandstone with occasional thin limestone beds; dolomite and anhydrite cement. Cross-lamination common. Interfingers with alluvial fans of Maroon Formation from Ancestral Rockies.	Majority eolian (intradune & extradune); minor fluvial
Entrada	Middle Jurassic	Fine-grained sandstone, mainly cross-bedded.	Eolian dunes, interdunes and sand sheets.
Dakota	Lower Cretaceous	Lower unit of fine- to coarse-grained sandstones with conglomeratic lenses; middle sand and shale unit; upper unit of sandstones and interbedded shales.	Lower, middle and portions of the upper unit are fluvial; the upper unit grades into extuarine or marginal marine deposits.

Uncertainty associated with the geology of the region is limiting the accuracy of both total CO_2 capacity and CO_2 injectivity (Bradshaw et al, 2007). Sparse data from the 233 oil and gas wells results in large areas where basic petrophysical data is lacking. Extrapolation/interpolation of down-hole geophysical data attempts to reduce the uncertainty where data is lacking, but the geophysical logs are also incomplete or inaccurate. Using the data from the on-going characterization project to calibrate down-hole logs with core-scale tests (porosity, permeability, injectivity, etc) of the injection and monitoring well will increase the accuracy of the logs from the region's other wells.

The Weber Sandstone is one of the major saline reservoirs that are present throughout the Colorado Plateau and Rocky Mountain basins, including the adjacent Piceance and Green River basins. The Weber Sandstone is estimated to have a storage potential of nearly 5 billion tons of CO_2 in Colorado, and potentially an equal amount from the same reservoirs in Utah, northeast Arizona, and northwest New Mexico [*DOE*, 2010; *NATCARB*, 2010]. Local and regional sources of CO_2 include the Craig coal-fired power plant and the Hayden coal-fired power plant approximately 35 km to the east of Craig, Colorado. The Craig and Hayden plants output at least 9.5 and 3.5 MMT of CO_2 per year, respectively [*NATCARB*, 2010].

The potential target formations in the proposed site are within a stacked aquifer system where shale and other fine-grained lithologies immediately overly the targeted injection formations. These low-permeability rocks act as localized seals. Additionally, a secondary sealing mechanism is created by the 3,500 feet thick Mancos Shale section that overlies the entire system.

The deepest saline aquifer, the Weber Formation, is overlain by thick (about 200 feet) Phosphoria Formation, a marine deposit comprised of shales, sandstones, limestones, dolomites and anhydrites. The Phosphoria Formation is considered the chief trap for the Rangely Field, a prolific Weber oil-producing field. Overlying the Phosphoria is approximately 900 feet of Triassic-age continental deposits of the Moenkopi and Chinle Formations. The Moenkopi and Chinle units are predominantly siltstones with minor conglomerates, sandstones and claystones, deposited in fluvial or lacustrine environments.

The Entrada Formation overlies the Chinle and is sealed by the Curtis Formation, a marine deposit consisting of shale, limestones and reworked Entrada sands with some oolites; it

averages 60 feet thick in the area of study. Overlying the Curtis Formation is the Morrison Formation, a Jurassic continental deposit consisting mostly of fluvial sands, silts and clays with some eolian dunes and lakebed deposits; the Morrison has an average thickness of 400 feet.

The Dakota Formation overlies the Morrison. It is sealed by the Mowry Shale, the lowermost shale deposited in the Cretaceous Seaway; it is a brittle marine shale about 90 feet thick. The Mowry is overlain by approximately 300 feet of the Frontier Formation, a coarsening upward marine deposit of shales and sandy shales grading upward to sands or shaly sands. 200 feet of Carlile Shale overlies the Frontier Formation; it is described as argillaceous siltstone and calcareous shale with some sands that were deposited in the Cretaceous Seaway.

Above the Carlile is the Niobrara Formation, a silty, calcareous shale targeted for potential unconventional injection. Overlying the Niobrara is 3,500 feet of Mancos Shale that was deposited in the Cretaceous Seaway. The Mancos consists of calcareous shale and argillaceous siltstone with some interbedded sands. Many impermeable layers are found within the Mancos minimizing risk of leakage if any of the lower primary seals should fail.

2.1. Geocelluar Model

Within the Sand Wash Basin, the stratigraphic formation top picks, well information, and well log images available from the project site were gathered to establish the geocellular model. Porosity values were assigned to the grid cells of the Dakota, Entrada and Weber Formations. This process began by taking porosity data from 20 existing wells within the Sand Wash Basin model boundary. Variogram analysis was conducted to understand the variation in porosity as a function of separation distance between existing wells. It was also used as means of determining directions/degree of anisotropy. Using the sample variogram results, Sequential Gaussian

Simulation (SGS) was used to assign porosity values to each cell within the Dakota, Entrada and Weber Formations of the Sandwash Basin.

In this study, the geocellular model (porosity) within the basin boundary shown in Figure 1 serves as a true geology. The constructed 3D model contains 6 formations starting with the Cretaceous Dakota formation to the Weber formation from top to bottom. The static model domain covers 107.7 miles by 58 miles in the x and y direction. The grid configuration is 569x306x26 cells in x, y, and z direction, respectively, with a cell dimension of 1,000 ft by 1,000 ft.
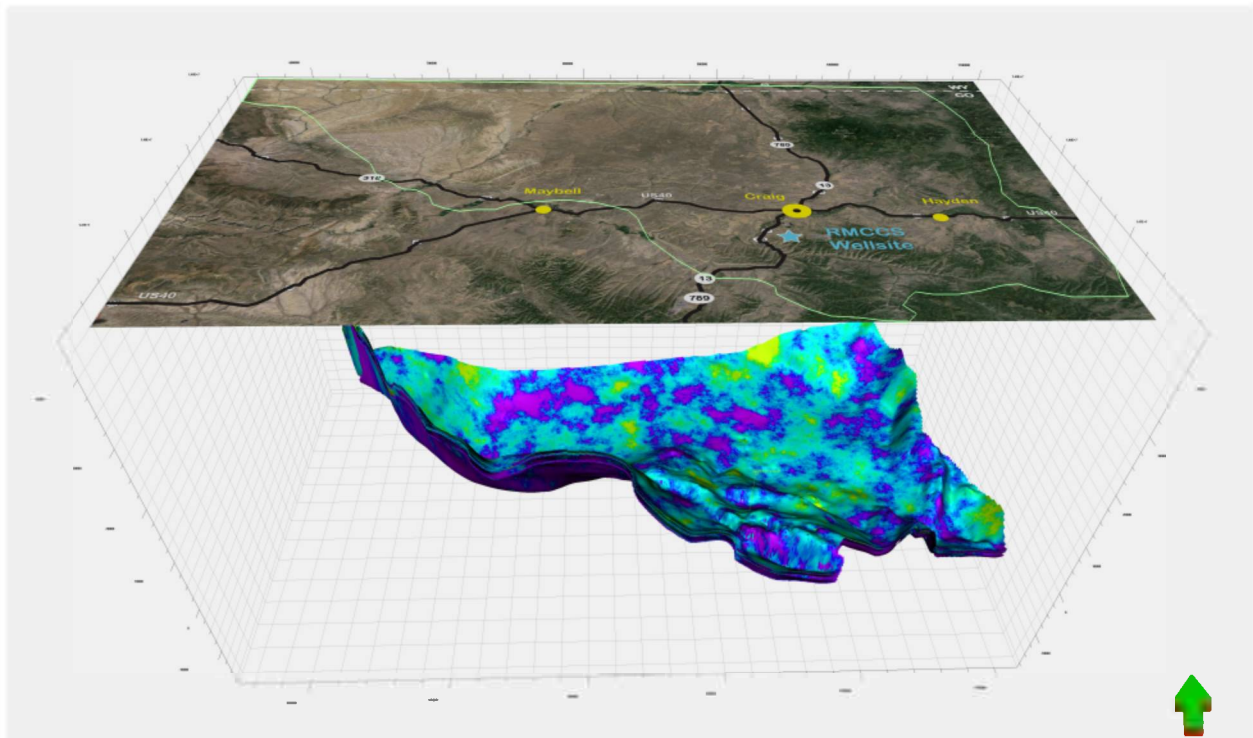
Figure 1. The Sand Wash Basin boundary and simulated porosity field within the boundary. Vertical exaggeration is 2x.

3. Methods

One newly drilled characterization well will provide good additional information on storage capacity; however, how close this new well progresses the project to understanding the true storage capacity estimate within the Sand Wash Basin is uncertain. It is also uncertain as to how many additional wells would be required to approach the true pore volume within the Basin. To understand this uncertainty a methodology was developed focusing on randomly placing "pseudo-wells" in a basin-scale model. Therefore, each randomly pseudo-well was assumed to provide new well data and additional geologic information. The recently developed geocelluar model of Sand Wash Basin was considered to be "true" or best estimate of real geology. We evaluated how the degrees of data density (well density) represented by the pseudo-wells affects the capacity estimates of target formations within the Sand Wash Basin. Note that we considered the estimated pore volume as a proxy to the capacity estimate in this work.

Figure 2 shows the general workflow we followed in this study. Based on the geocellular model of Sand Wash Basin, for 25 individual cases, we randomly sampled the location of pseudo-wells (or new characterization well) up to 25 within the model. As each well was placed, porosity and formation thickness information within each well was extracted from the Sand Wash Basin geocellular model which is considered to be "true" or best estimate of real geology. Starting from a first randomly sampled point, we sequentially added a new pseudo-well into the previous well(s) and calculated the estimated pore volume at each step to see how the new information affects the capacity estimates. That is, addition of pseudo-well(s) is supposed to provide additional information within the Sand Wash Basin.

```
┌─────────────────────────┐              ┌─────────────────────────┐
│ Sand Wash Basin         │              │ True (or best) estimate │
│ and/or small-scale model│─────────────▶│                         │
│ (geocellular model)     │              └─────────────────────────┘
└─────────────────────────┘
            │
            ▼
┌─────────────────────────┐
│ Random pseudo-well      │
│ sampling                │              ┌─────────────────────────┐
│ (Fm tops, porosity logs)│              │ Increase the # of       │
└─────────────────────────┘              │ pseudo-wells            │
            │                            └─────────────────────────┘
            ▼
┌─────────────────────────┐
│ Estimate storage        │
│ capacity                │
│ (geocellular model,     │
│  GIS, or ?)             │
└─────────────────────────┘
            │
            ▼
┌─────────────────────────┐
│ Compare the results     │
│ w/ true value           │
└─────────────────────────┘
            │
            ▼
        ◇ Satisfied ? ◇──────────────────────────────────
            │
            ▼
      ┌──────────┐
      │ Results  │
      └──────────┘
```
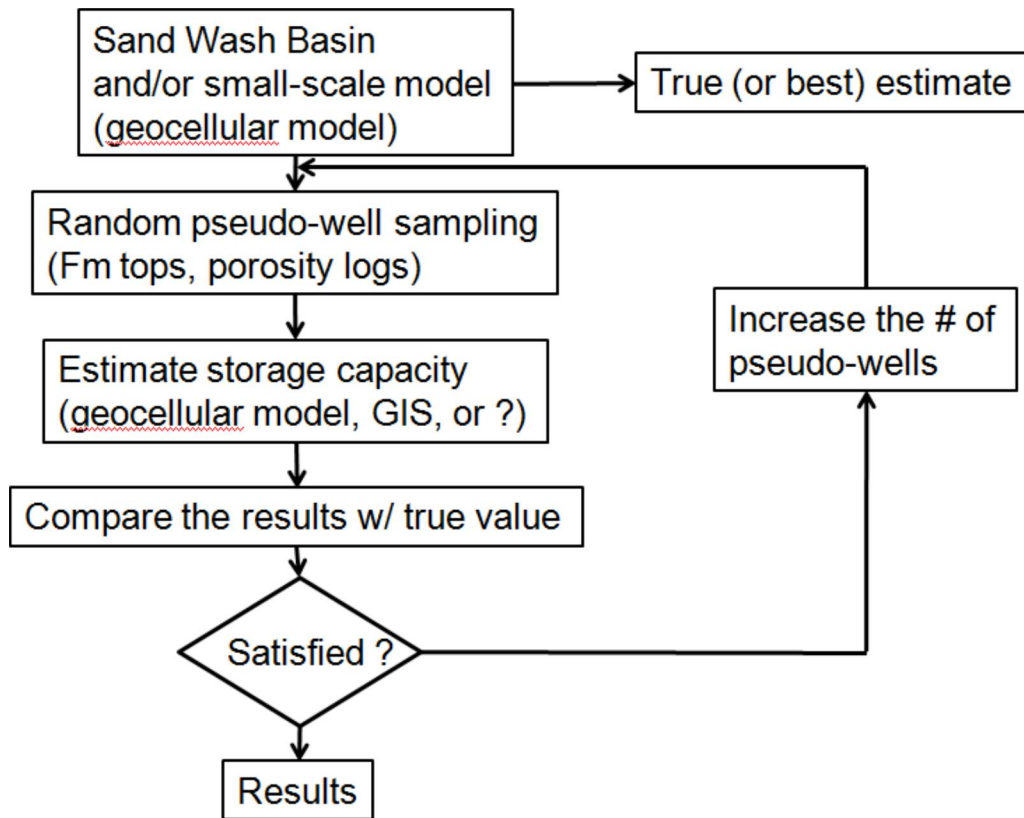
Figure 2.   Workflow for the pore volume estimation with the incremental addition of pseudo-well.

Average porosity value and thickness of a target formation were determined from each pseudo-well and assigned uniformly to the subarea corresponding to the pseudo-well. The estimated pore volume of a subarea was simply computed by the product of average porosity value, thickness, and size of the subarea. For example, Figure 3 shows 25 subareas of Dakota formation corresponding to the randomly selected 25 pseudo wells for case 1. The boundary of each subarea was determined by the closest distance from each pseudo-well. Total estimated pore volume of the basin is the sum of each subarea's estimated pore volume. We repeated the same process for a total of 25 cases with a different starting pseudo-well location for statistical analysis. As an example, Appendix A summarizes the change in the subareas corresponding to

the selected number of wells in case 1. Appendix B also includes the final areal division (25 subareas) for the case 2 – 25.
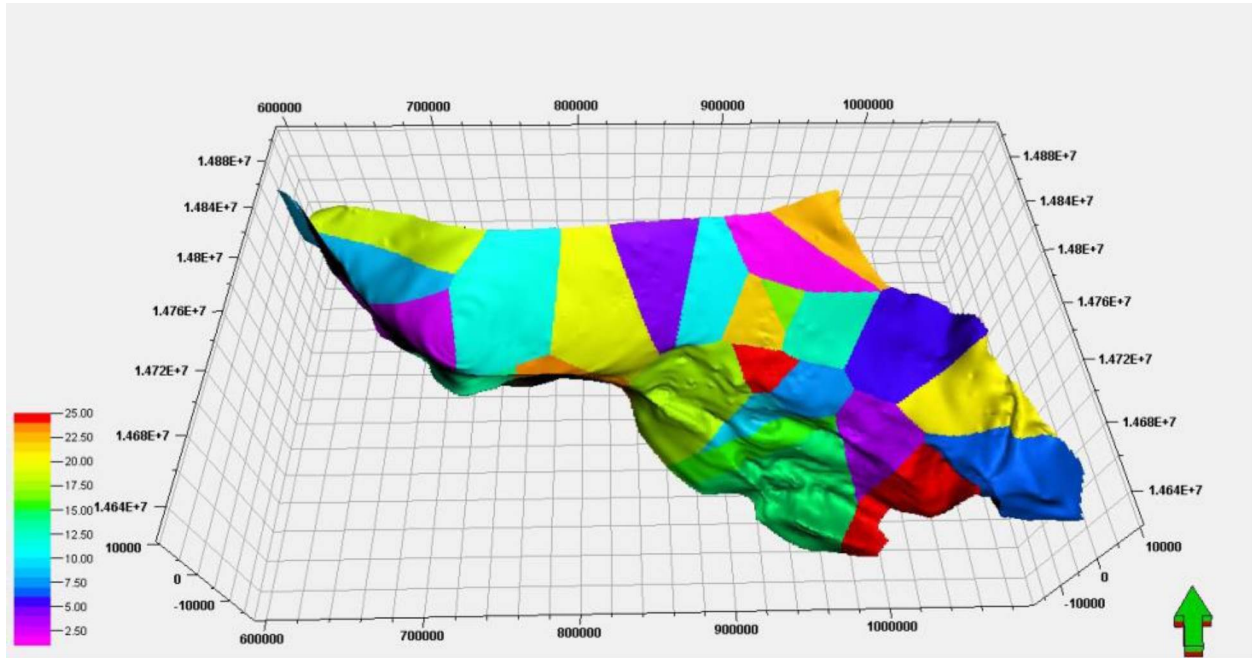
Figure 3. Case 1, 25 subareas applied in the Dakota formation based on the closest point from corresponding pseudo wells within the Sand Wash Basin. For this method, 24 other cases like the above were run and produced alternate data sets. Vertical exaggeration is 2x.

4. Results and Discussion

Figures 4-6 show the obtained relative differences of the capacity estimates from the true value of geocellular model for Dakota, Entrada, and Weber formation, respectively for cases 1-25. The relative difference is defined by $\frac{V_{est}-V_{true}}{(V_{est}+V_{true})/2}$ where V_{est} is the estimate of total pore volume and V_{true} is the true capacity value from the geocellular model. That is, if the relative difference reaches zero, the pore volume (or storage capacity) estimate is close to the true value. Positive relative difference represents the overestimation and negative value is underestimation to the true value.
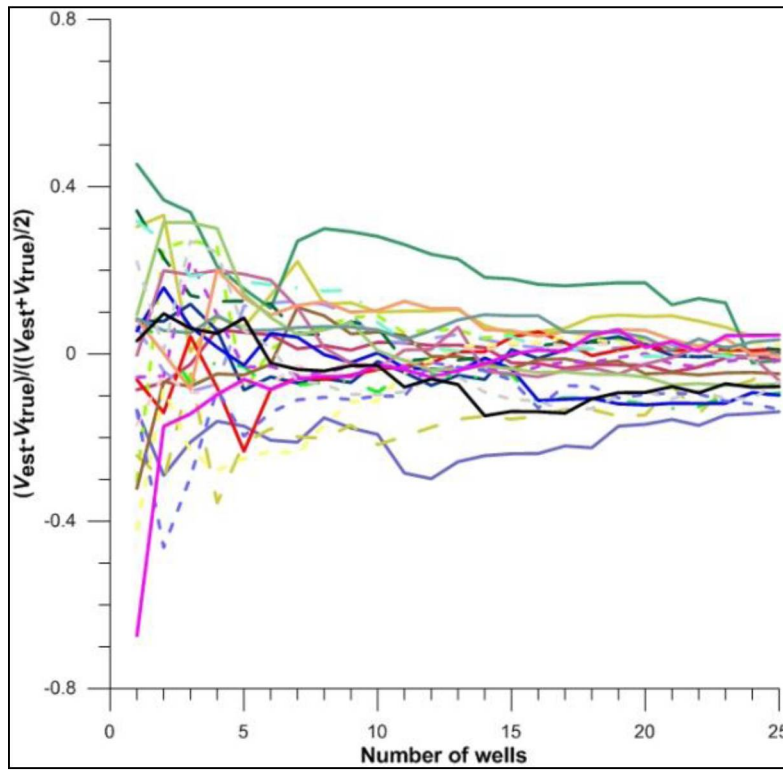
Figure 4. Case 1-25 combined data set, relative differences of the capacity estimates from the true value of geocellular model for Dakota formation. Each line represents 1 of the 25 cases.
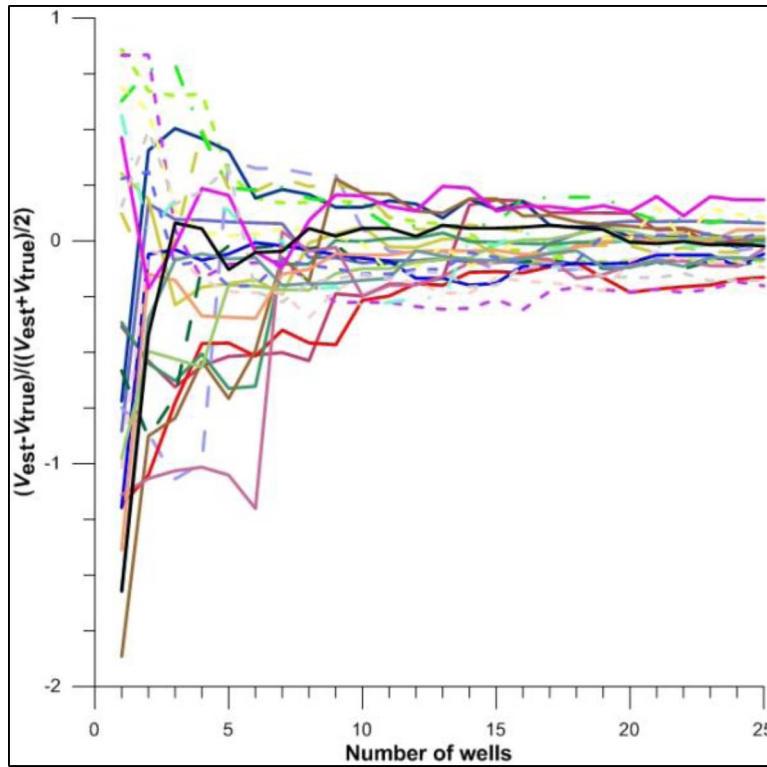
Figure 5. Case 1-25 combined data set, relative differences of the capacity estimates from the true value of geocellular model for Entrada formation. Each line represents 1 of the 25 cases.
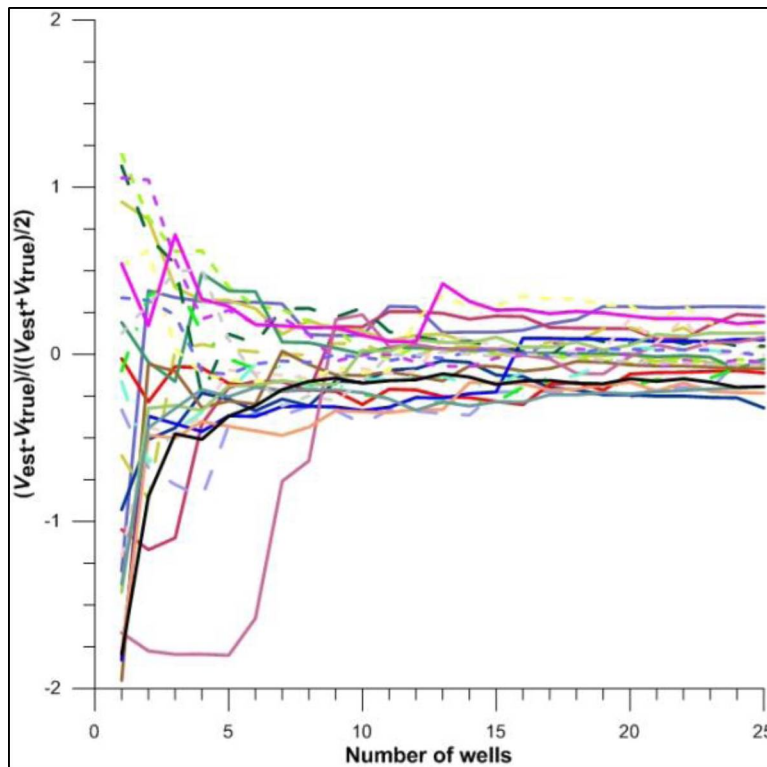
Figure 6. Case 1-25 combined data set, relative differences of the capacity estimates from the true value of geocellular model for Weber formation. Each line represents 1 of the 25 cases.

As expected, our results show that the difference between the estimated pore volume and true value is decreasing with the addition of new data (pseudo-wells) (Figures 4 – 6). However, pore volume estimation for the Dakota (Figure 4) shows better fit especially with less number of pseudo-wells compared to Entrada and Weber formation (Figures 5 and 6). Since the estimated pore volume of a subarea is computed with the single porosity and thickness value given by the corresponding pseudo-well, the difference will increase if there is a large spatial variation in the porosity and thickness within a subarea. In other words, our results indicate that Dakota formation has relatively less spatial variation in the porosity and thickness. Targeting ±30% relative difference as a tolerable error range, our results show that we would need at least 5 and 9

characterization wells for the Dakota and 9 wells for Entrada and Weber formations, respectively. Note that appropriate density of characterization data/well is dependent on the geologic formations even within the same basin.

With the minimum, lower quartile, median, upper quartile, and maximum, Box-Whisker plots shown in Figures 7 – 9 graphically summarize the results for cases 1-25 of the pore volume estimates (relative difference) at different number of pseudo-wells for the Dakota, Entrada, and Weber, respectively. The bottom of the box is the 25th percentile and the top is 75th percentile. The horizontal line within the box shows the median value and the end of whiskers are the minimum and maximum. The range/distribution of relative difference value for the small number of wells is significantly larger for the Entrada and Weber formation compared to the Dakota. Even with the single characterization well, median of relative difference out of 25 cases is close to zero. Whereas, the Entrada and Weber formation exhibited large negative median (underestimation) with a single characterization well and gradually decreased the difference as the number of wells increased.
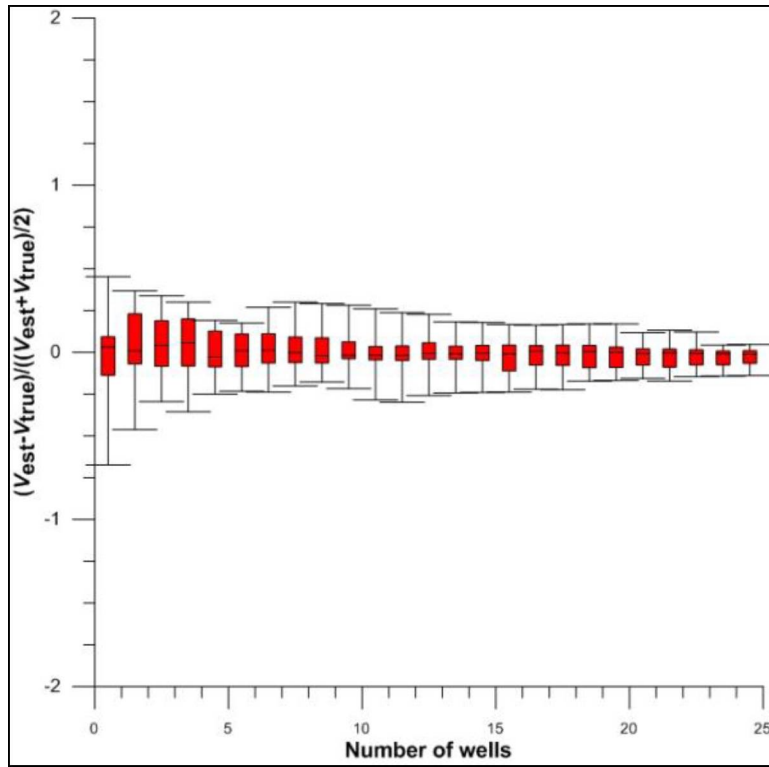
Figure 7. Case 1-25 combined data set, Box-Whisker plot of the relative difference of the capacity estimates for Dakota formation from the true value of geocellular model.
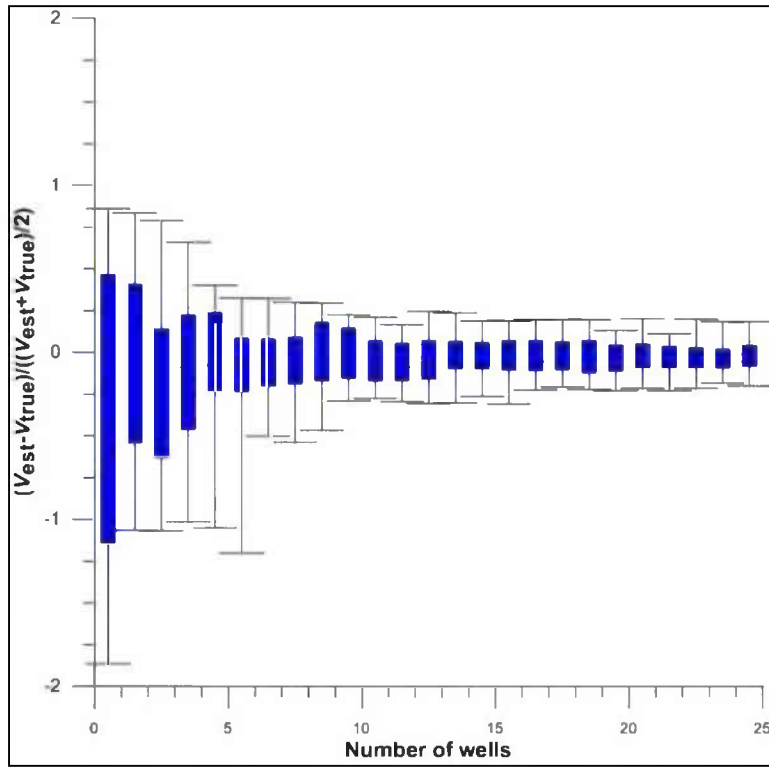
Figure 8.   Case 1-25 combined data set, Box-Whisker plot of the relative difference of the capacity estimates for Entrada formation from the true value of geocellular model.
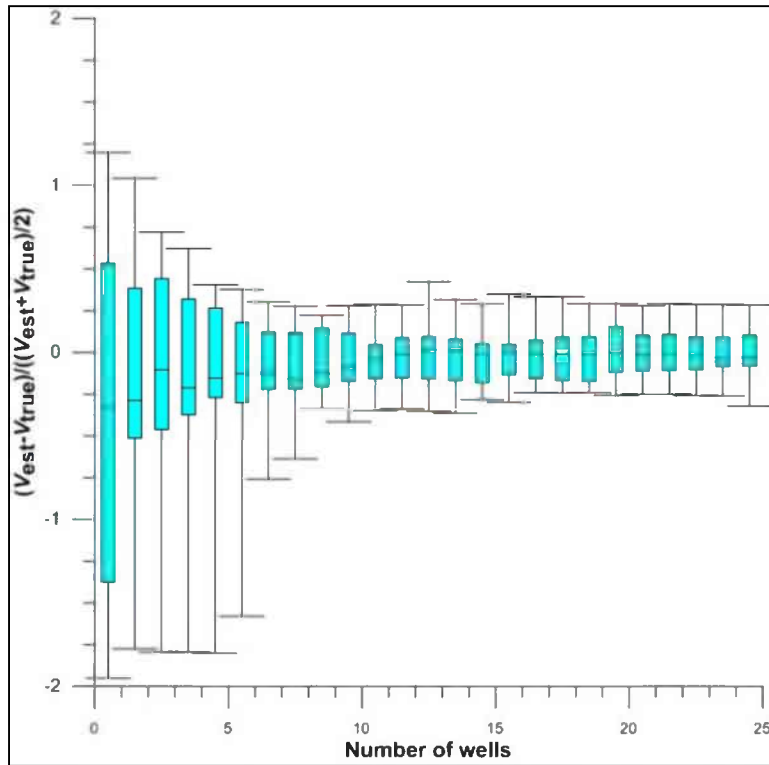
Figure 9.   Case 1-25 combined data set, Box-Whisker plot of the relative difference of the capacity estimates for Weber formation from the true value of geocellular model.

As our relative difference measurement shows the deviation from the true value, we also analyzed which factor is more significant in terms of pore volume estimation. Note that our pore volume estimates in this work involves the uncertainties only in porosity and cell volume (geometry of geologic structures). To adequately quantify the degree of variation in the geologic structures and its effect on the capacity estimation, we calculated volume-weighted average dip angle of each target formation. Being consistent with our relative difference measurements, the volume-weighted dip angle for the Dakota is the smallest (4.95 degrees) among three target formations (Table 2).   Entrada and Weber are characterized by higher volume-weighted dip angle of 11.32 and 9.49 degrees, respectively. That is, a formation with a large dip angle is

likely to have more uncertainty and greater error in the capacity estimation with the limited characterization data. However, unlike the volume-weighted average dip angle, the degree of heterogeneity in the porosity was not consistent with our relative difference results. Table 2 summarizes the general statistics of the porosity from the original well logs and simulated true porosity field.

Table 2. Volume-weighted average dip angle and general statistics of porosity field.

		Dakota	*Entrada*	*Weber*
Volume-weighted average dip angle		4.95	11.32	9.49
Minimum	Property	0.0165	0.0163	0.015
	Well Logs	0.015	0.015	0.015
Maximum	Property	0.1434	0.1364	0.0722
	Well Logs	0.3706	0.1558	0.1168
N	Property	89173	88549	88862
	Well Logs	2886	2366	840
Mean	Property	0.0637	0.0468	0.0297
	Well Logs	0.0667	0.0517	0.0342
Std. Dev.	Property	0.0172	0.02	0.0136
	Well Logs	0.0365	0.0247	0.021

Although our results did not consider the cost analysis in this study, greater characterization efforts and cost should be accounted for the reliable capacity estimates in the Entrada and Weber due to their more complicated spatial variation in geology and/or petrophysical properties. Our findings demonstrate with confidence that spatial geologic variation strongly affects the capacity estimation and associated uncertainty.

Although our results did not consider the cost analysis in this study, greater characterization efforts and cost should be accounted for the reliable capacity estimates in the Entrada and Weber due to their more complicated spatial variation in geology and/or petrophysical properties.   Our findings demonstrate with confidence that spatial geologic variation strongly affects the capacity estimation and associated uncertainty.

References

Bradshaw, J., et al. (2007), CO2 storage capacity estimation: Issues and development of standards, *International Journal of Greenhouse Gas Control*, *1*(1), 62-68.

DOE (2010), Carbon Sequestration Atlas of the United States and Canada, edited, U.S. Department of Energy, Office of Fossil Energy, National Energy Technology Laboratory.

IPCC (2007), The Physical Science Basis. Contribution of Working Group I to the Fourth Assessment Report of the Intergovernmental Panel on Climate Change, 996 pp.

NATCARB (2010), National Carbon Sequestration Database and Geographic Information System, edited.

Appendix

A.   Subareas in the case 1 based on the closest point from corresponding selected pseudo wells within the Sand Wash Basin

B.   Final areal division (25 subareas) of case 2 – 25.
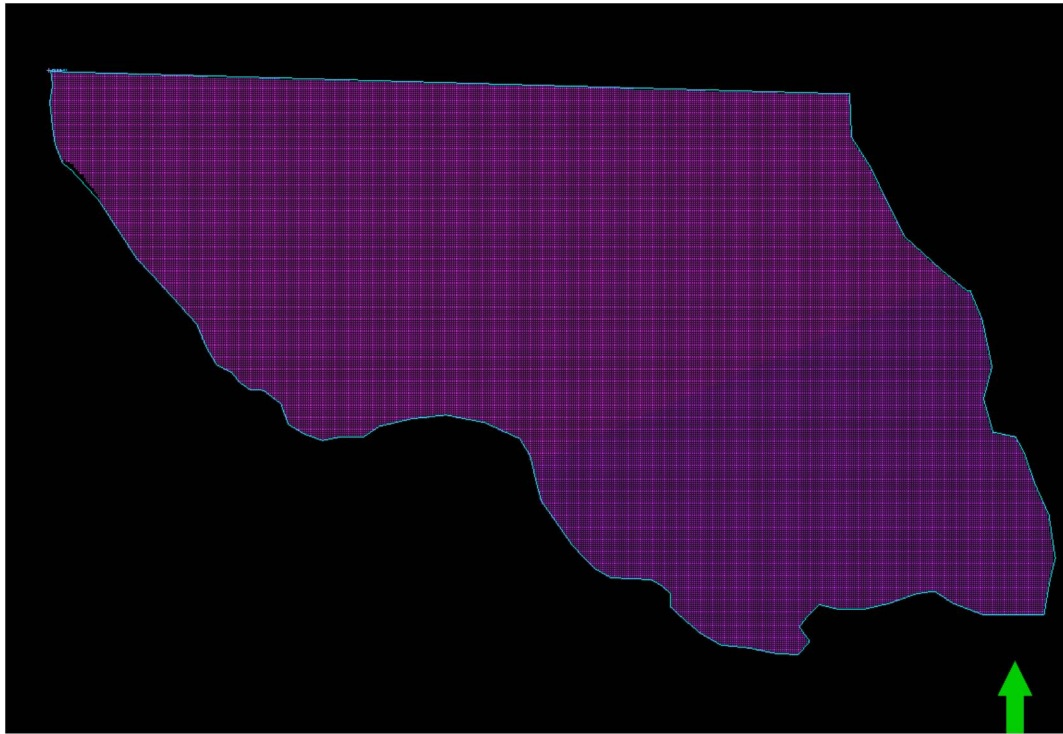
A1. 2 subareas of case 1.
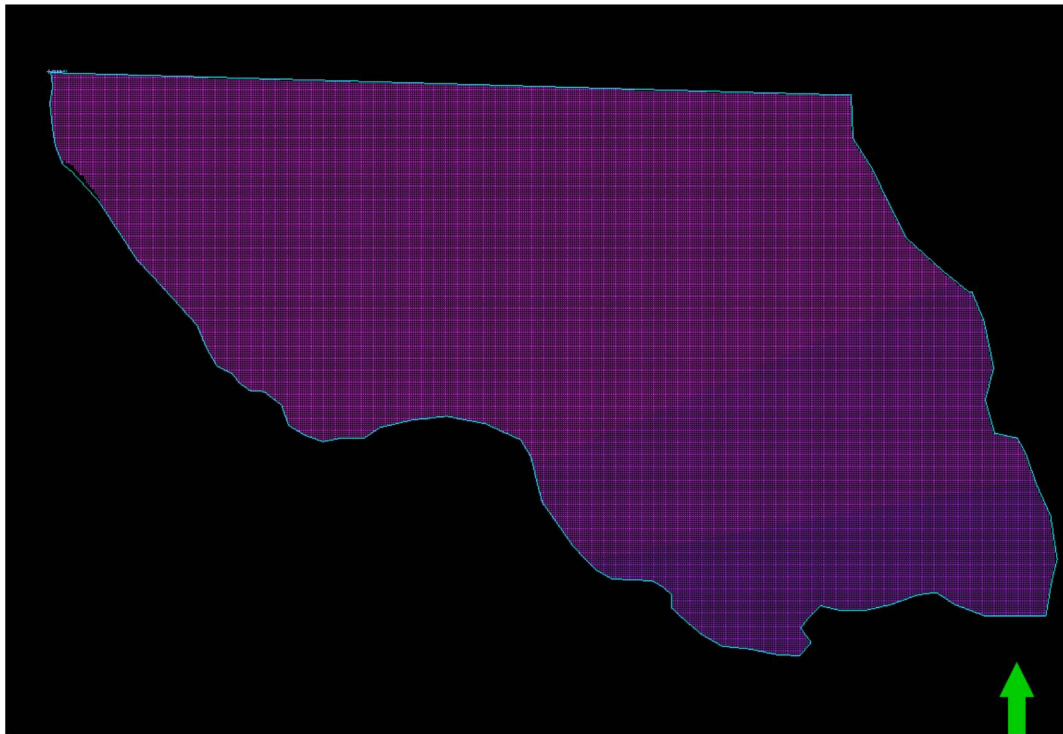
A2. 3 subareas of case 1.
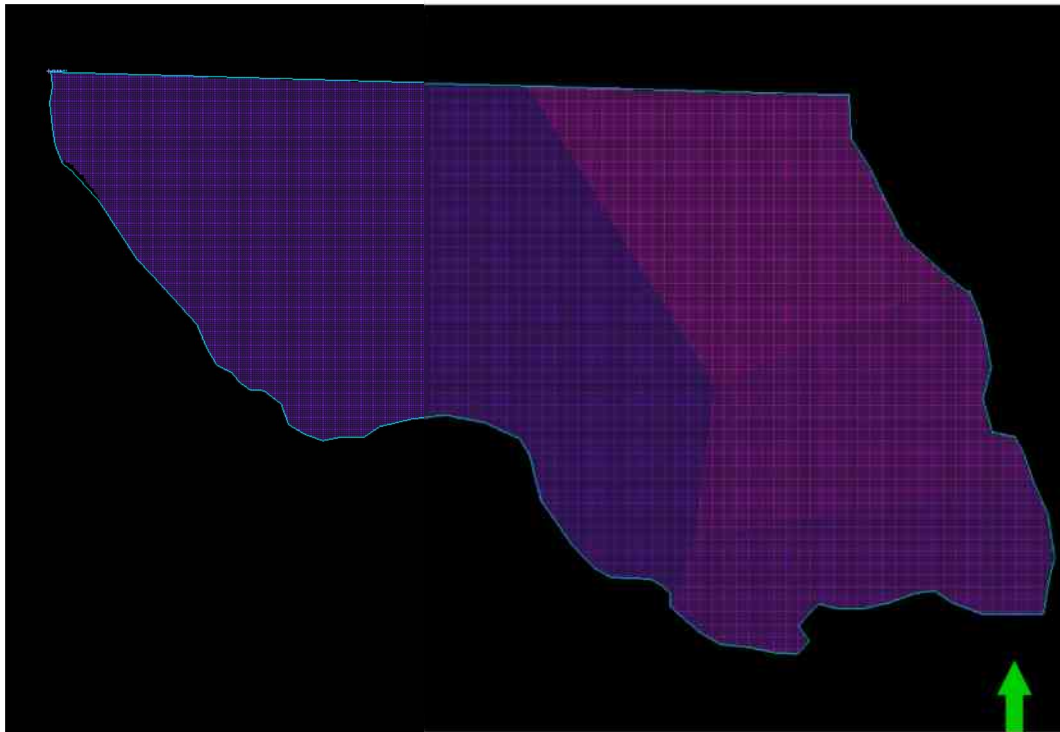
A3. 4 subareas of case 1.
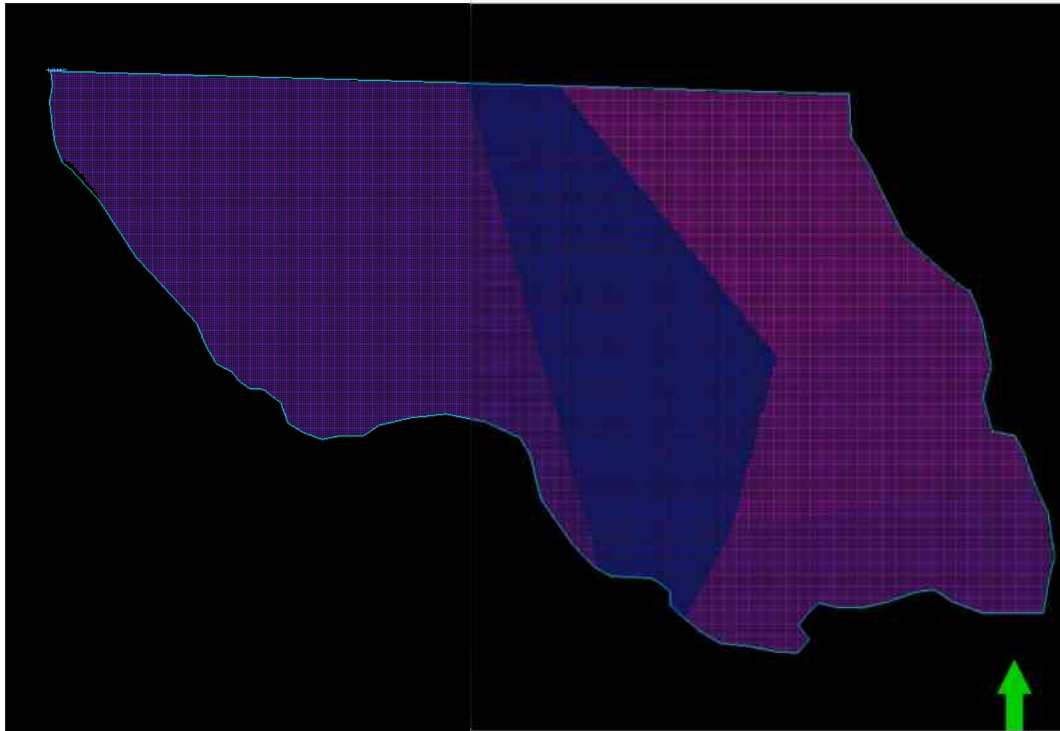
A4. 5 subareas of case 1.
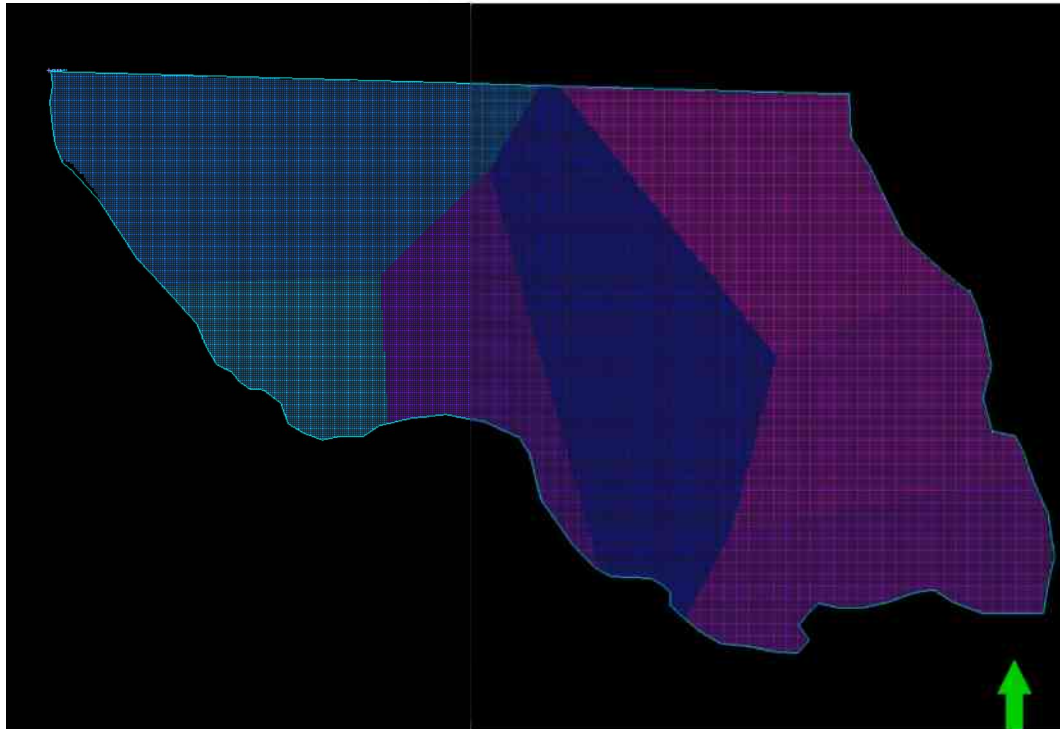
A5. 7 subareas of case 1.
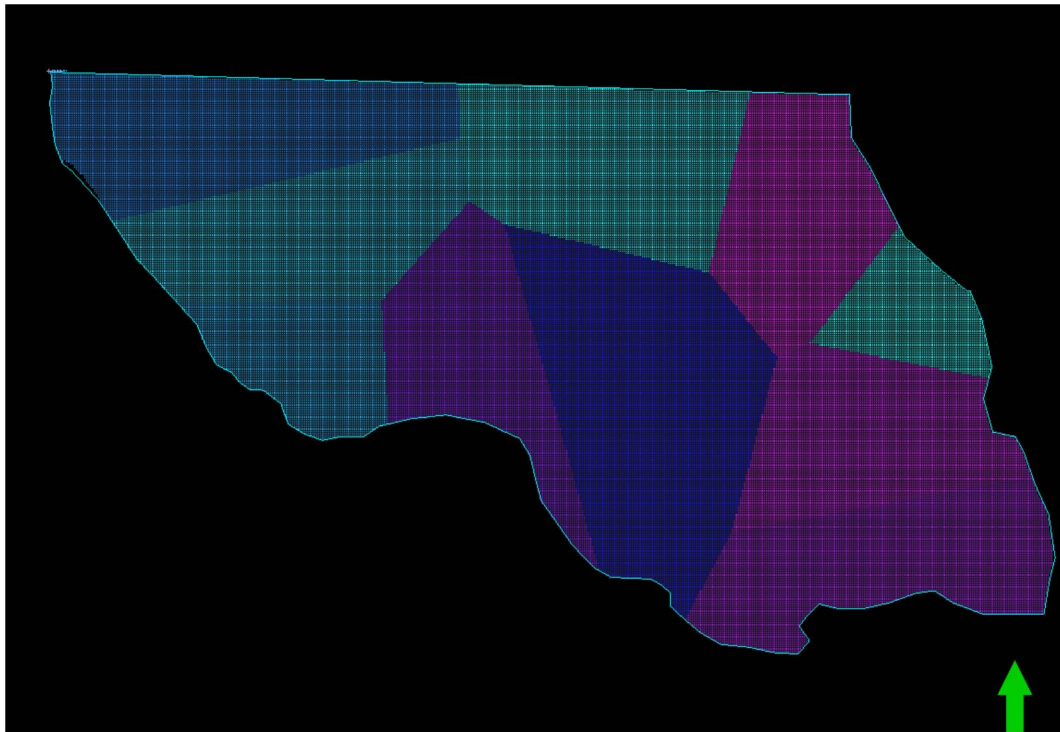
A6. 10 subareas of case 1.
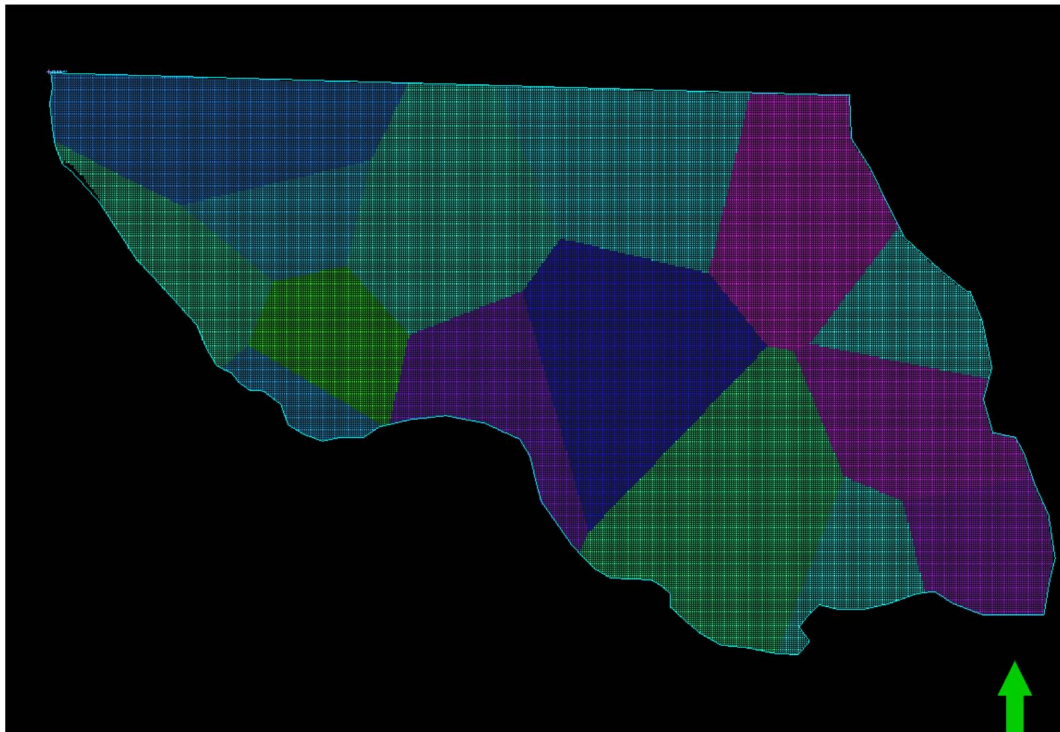
A7. 15 subareas of case 1.
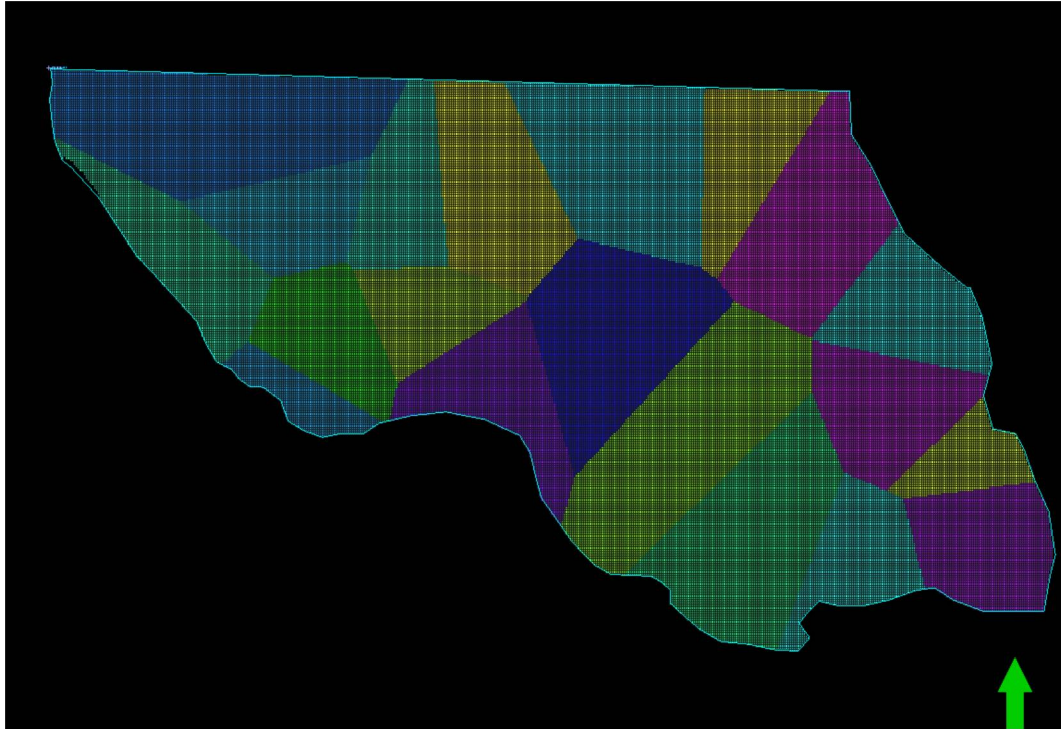
A8. 20 subareas of case 1.
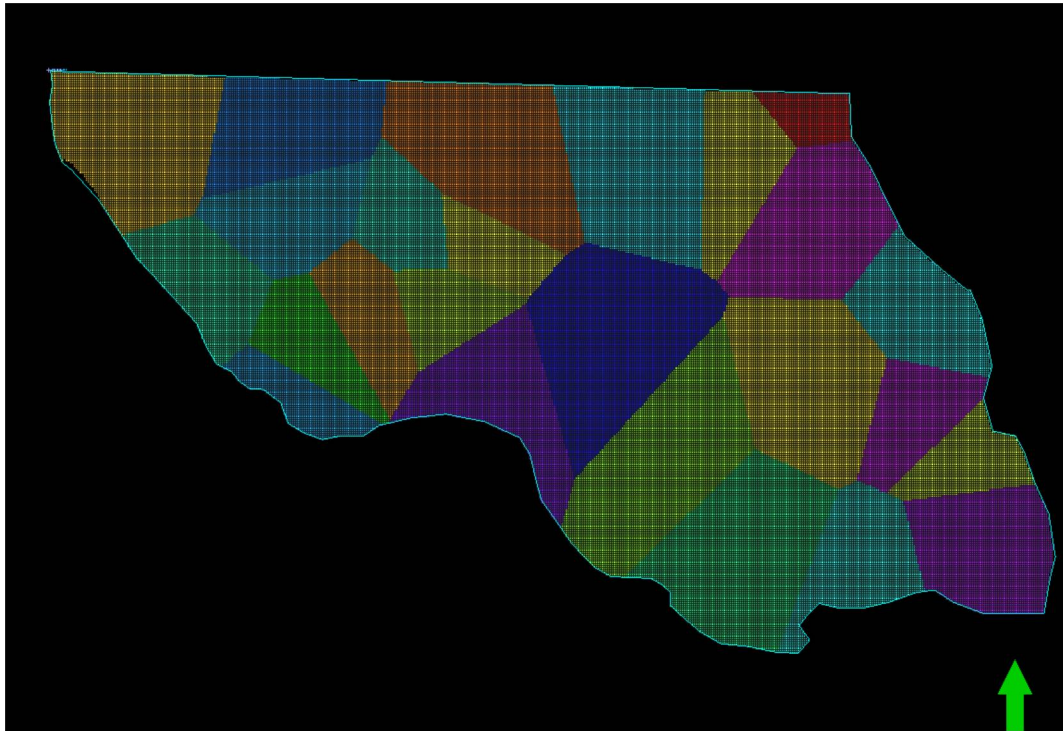
A9. 25 subareas of case 1.
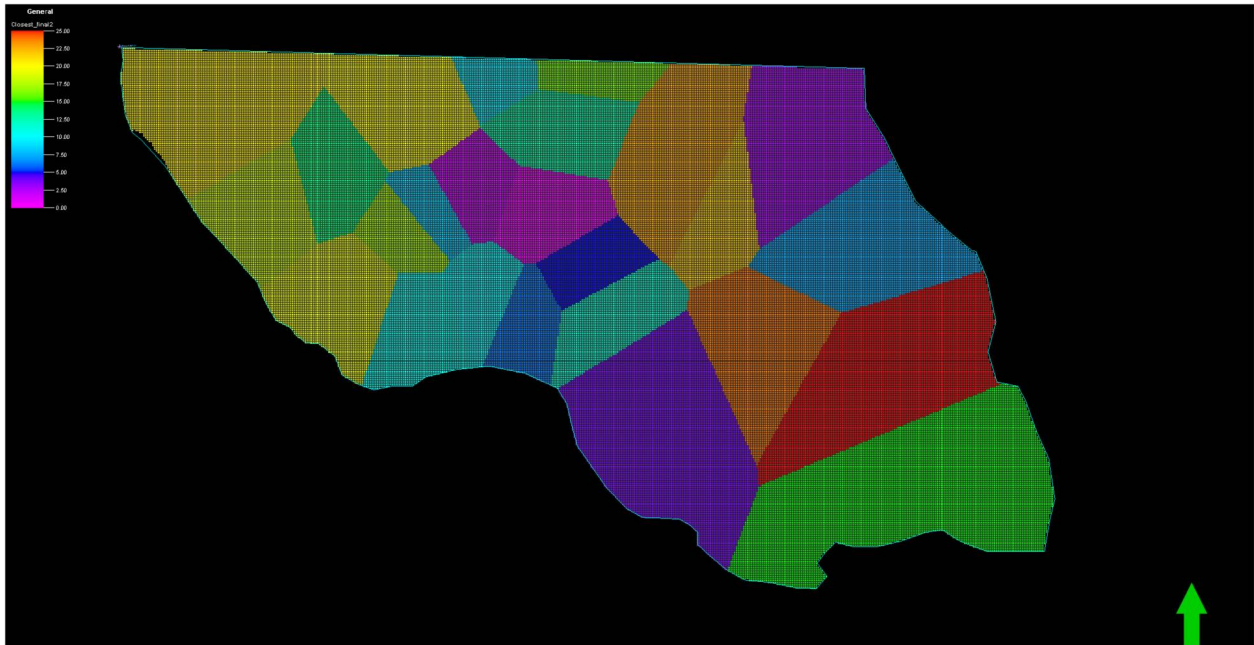
B1. Final areal division (25 subareas) corresponding to 25 pseudo wells in case 2.
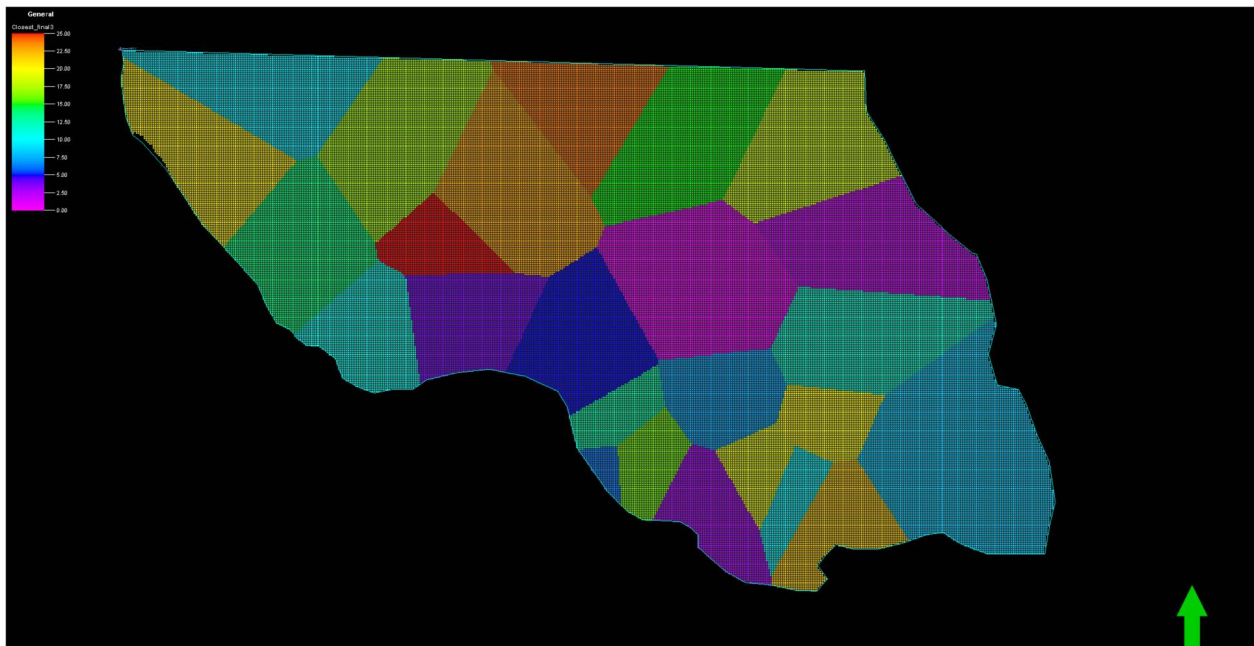
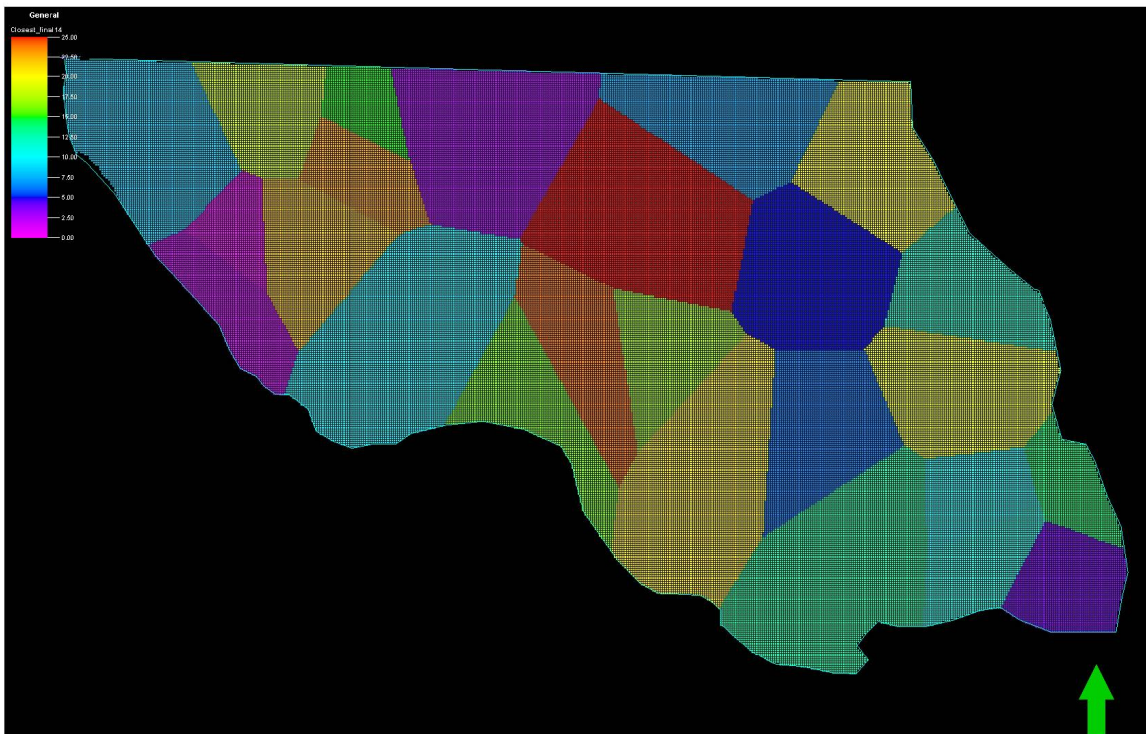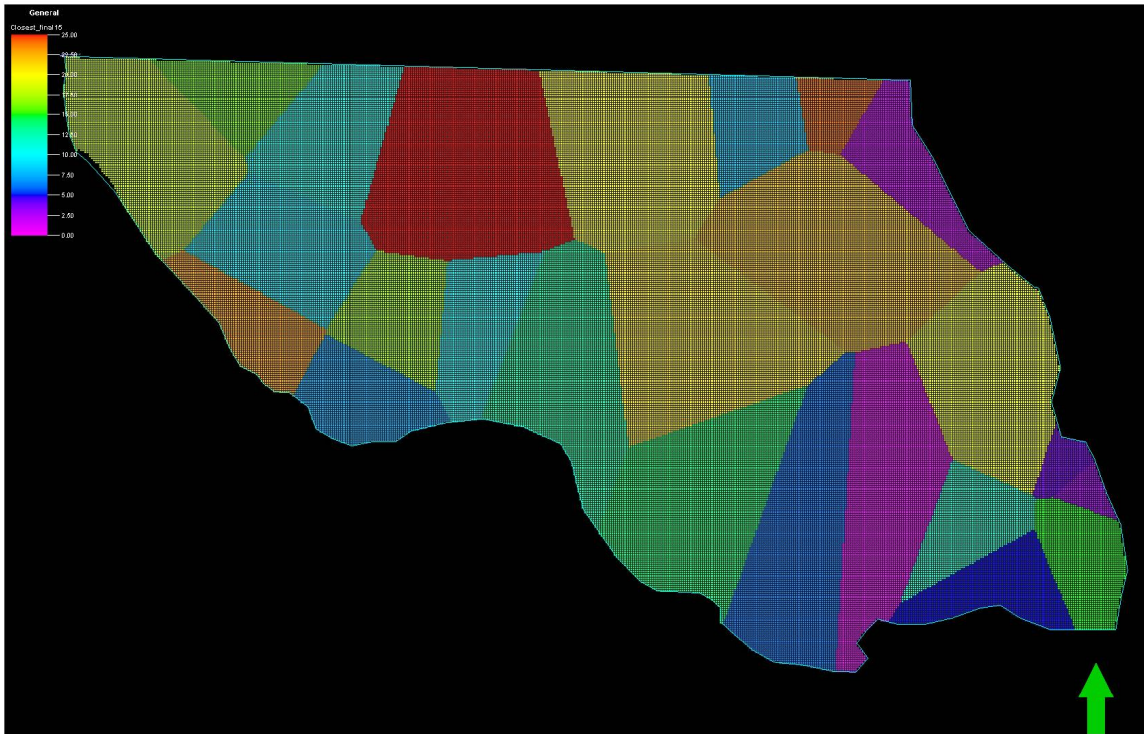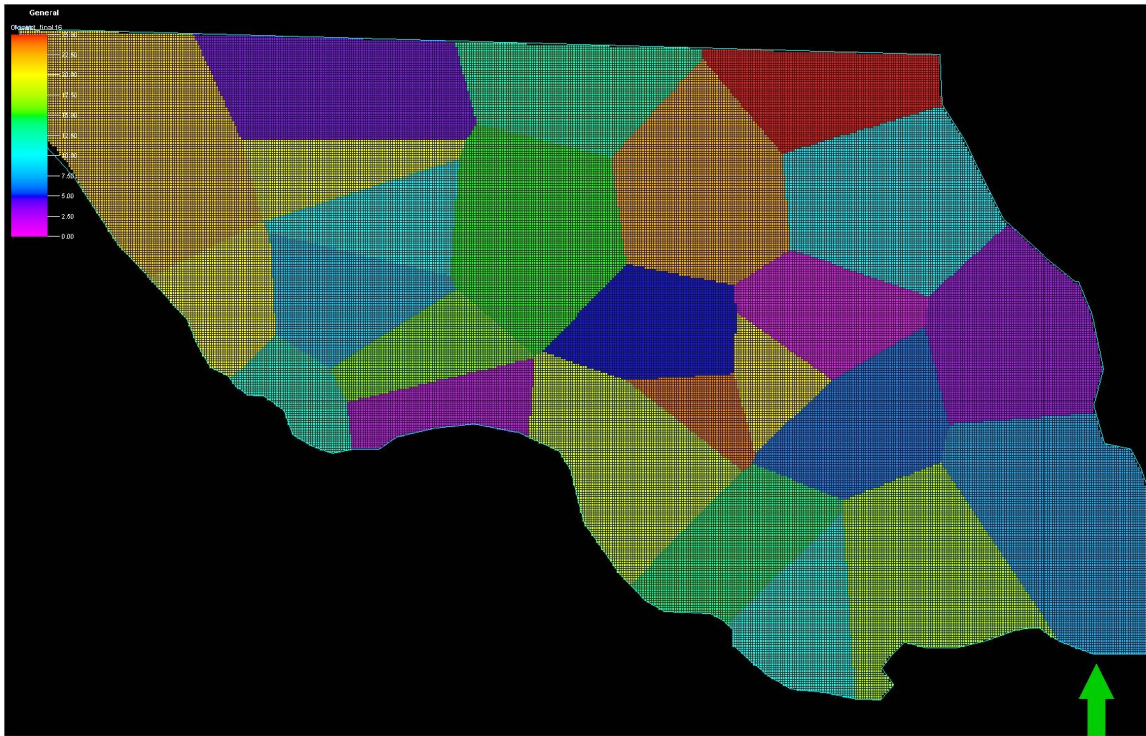B2. Final areal division (25 subareas) corresponding to 25 pseudo wells in case 3.
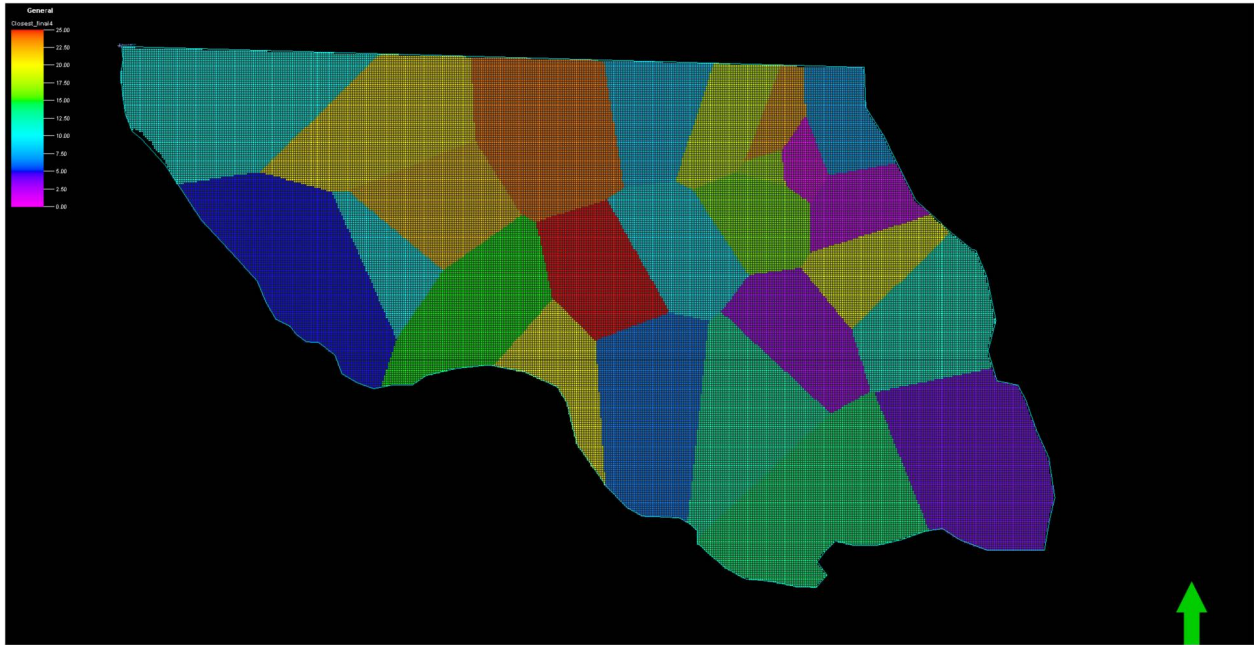
B3. Final areal division (25 subareas) corresponding to 25 pseudo wells in case 4.
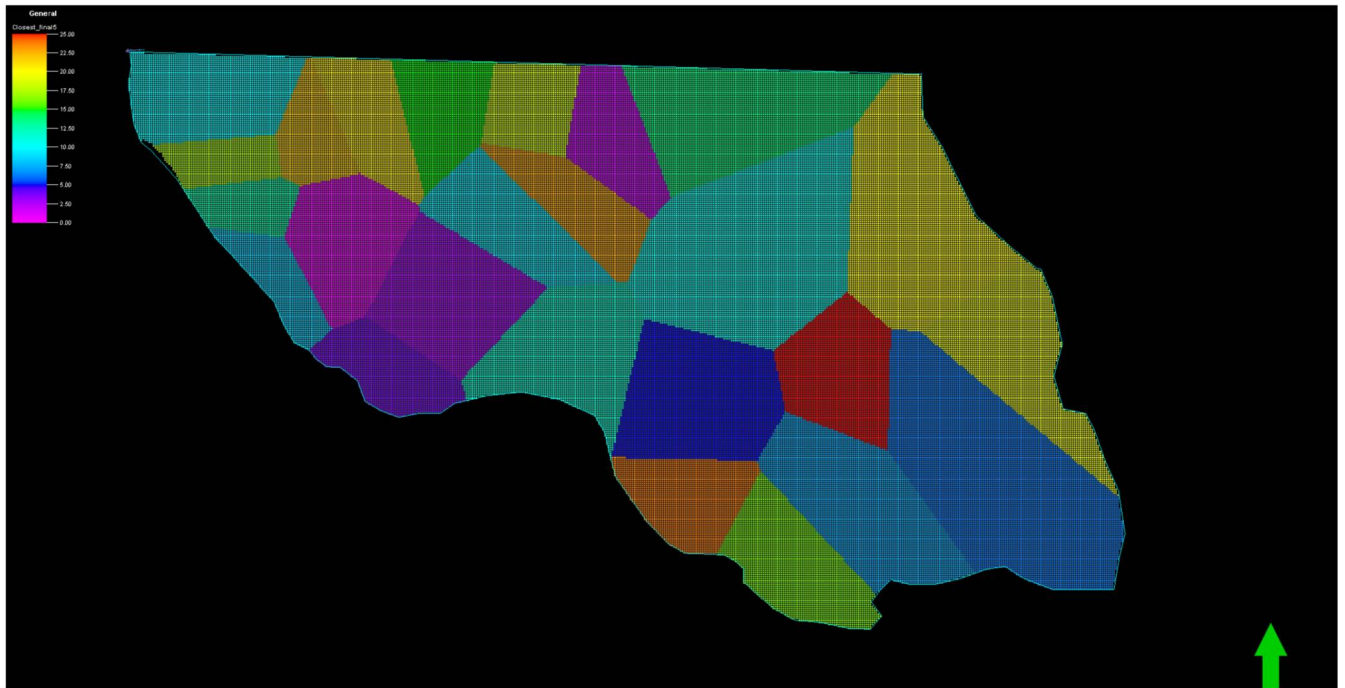
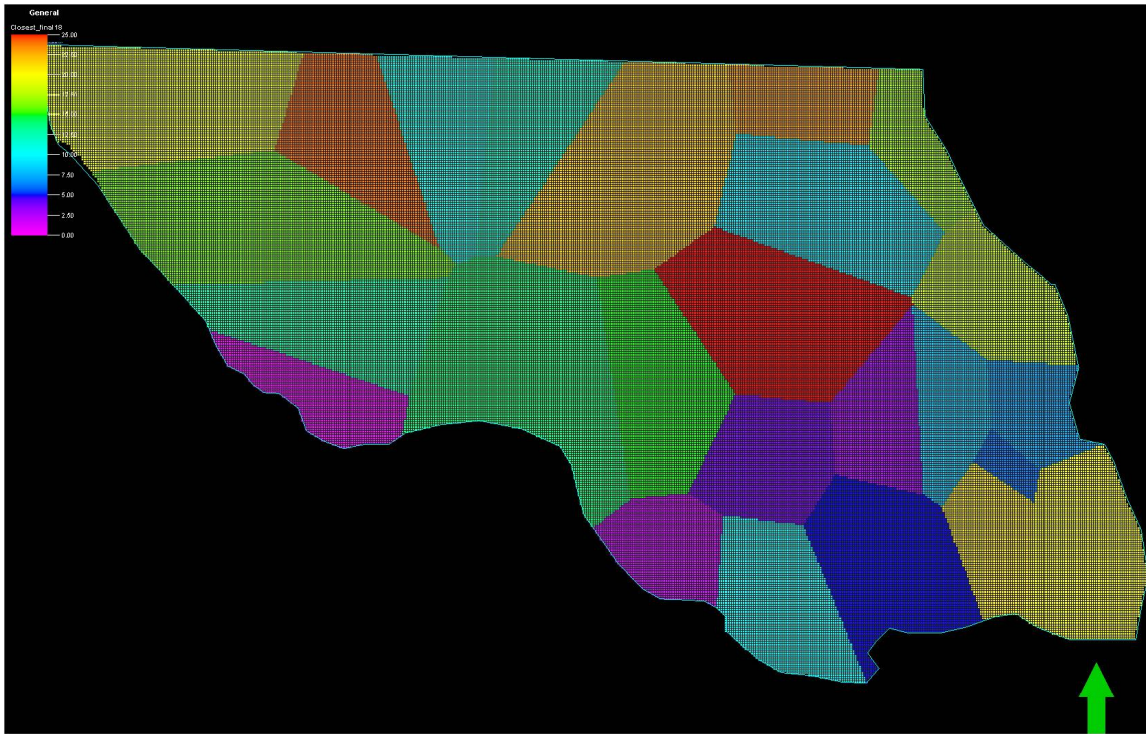B4. Final areal division (25 subareas) corresponding to 25 pseudo wells in case 5.
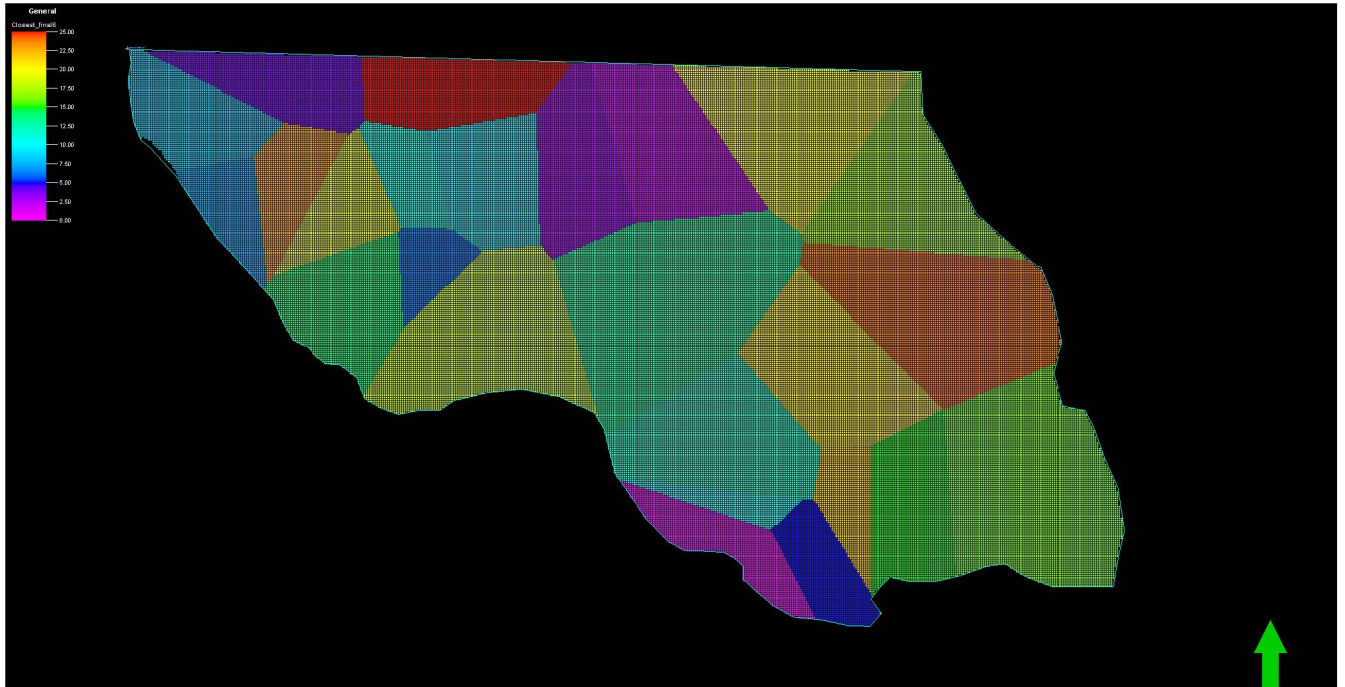
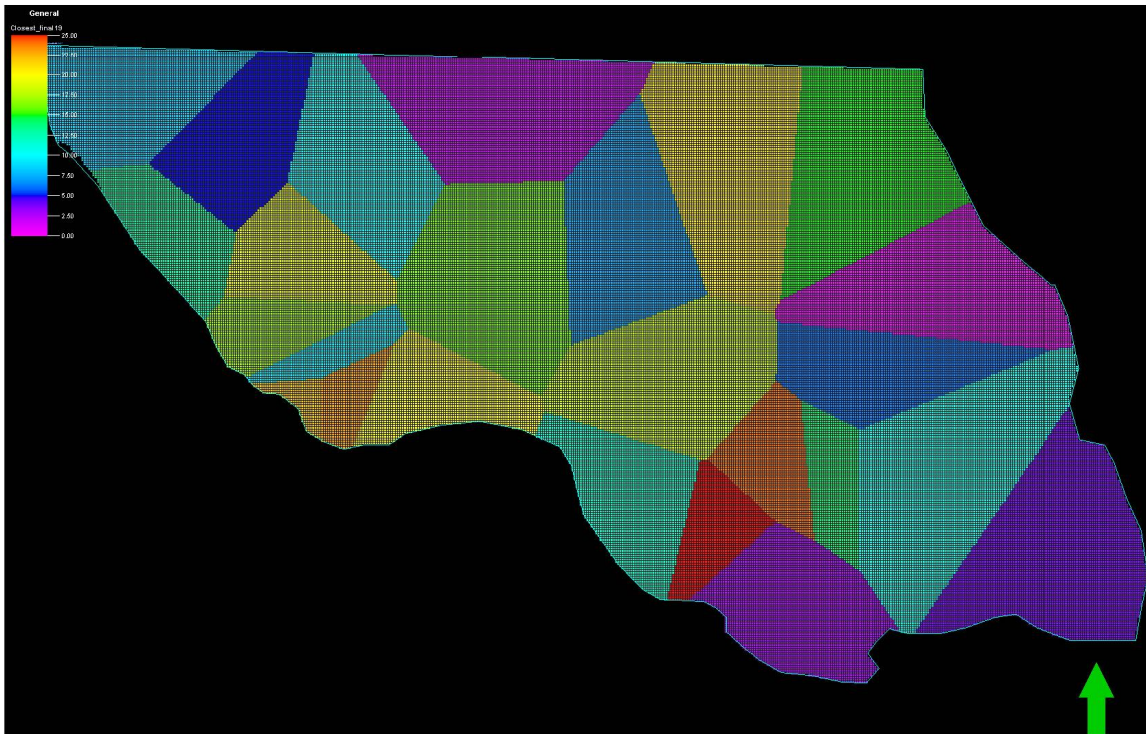B5. Final areal division (25 subareas) corresponding to 25 pseudo wells in case 6.
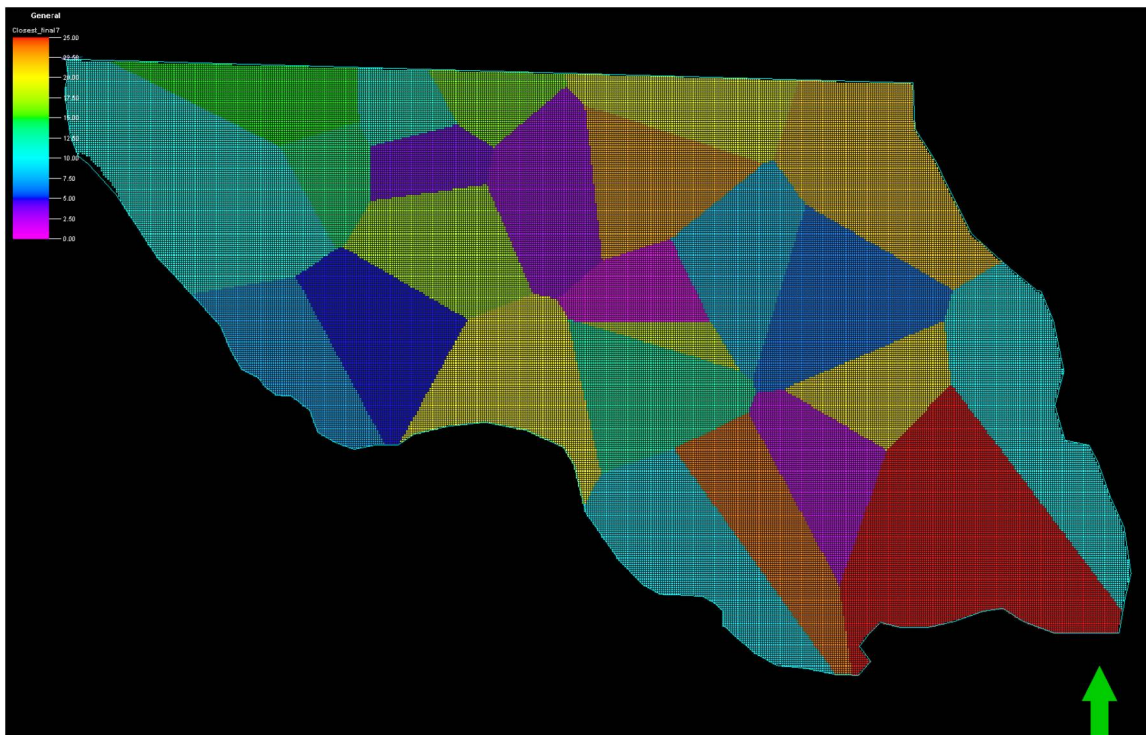
B6. Final areal division (25 subareas) corresponding to 25 pseudo wells in case 7.
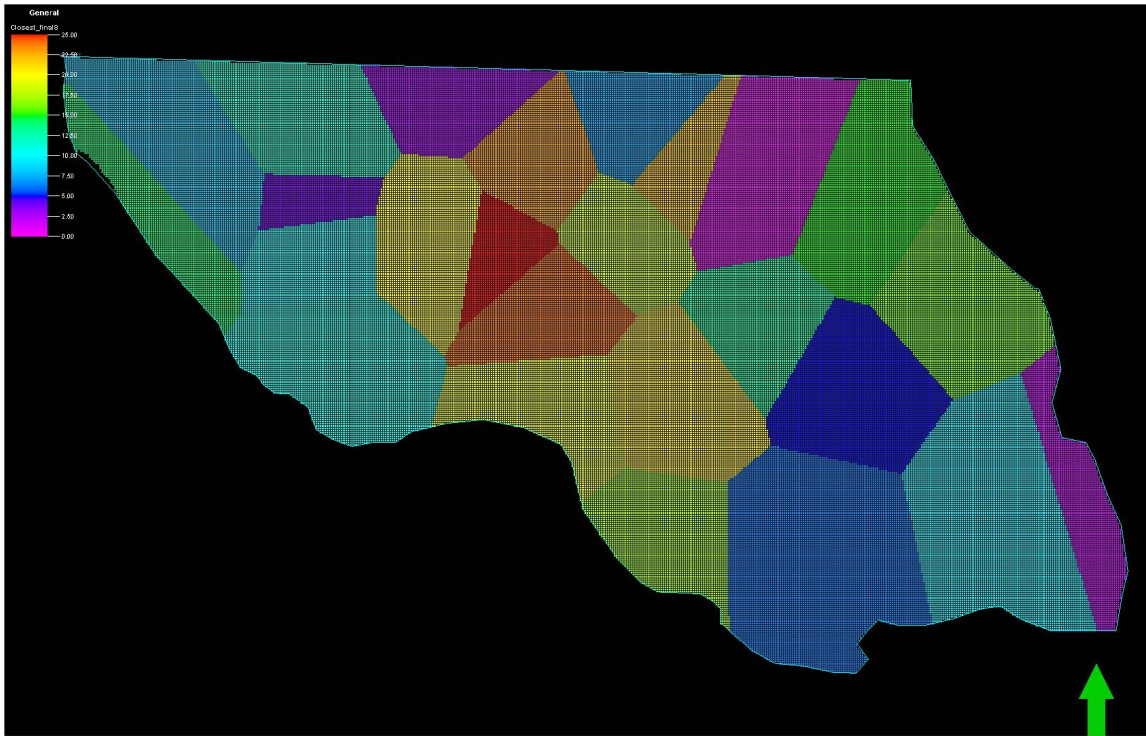
B7. Final areal division (25 subareas) corresponding to 25 pseudo wells in case 8.
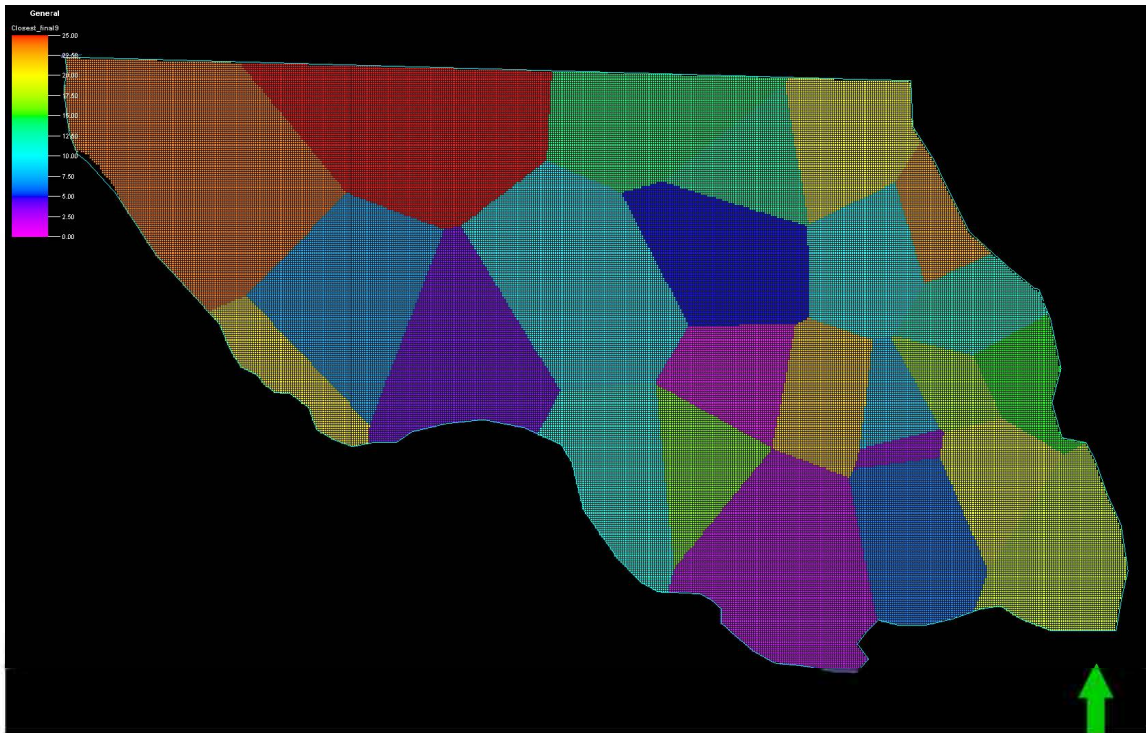
B8. Final areal division (25 subareas) corresponding to 25 pseudo wells in case 9.
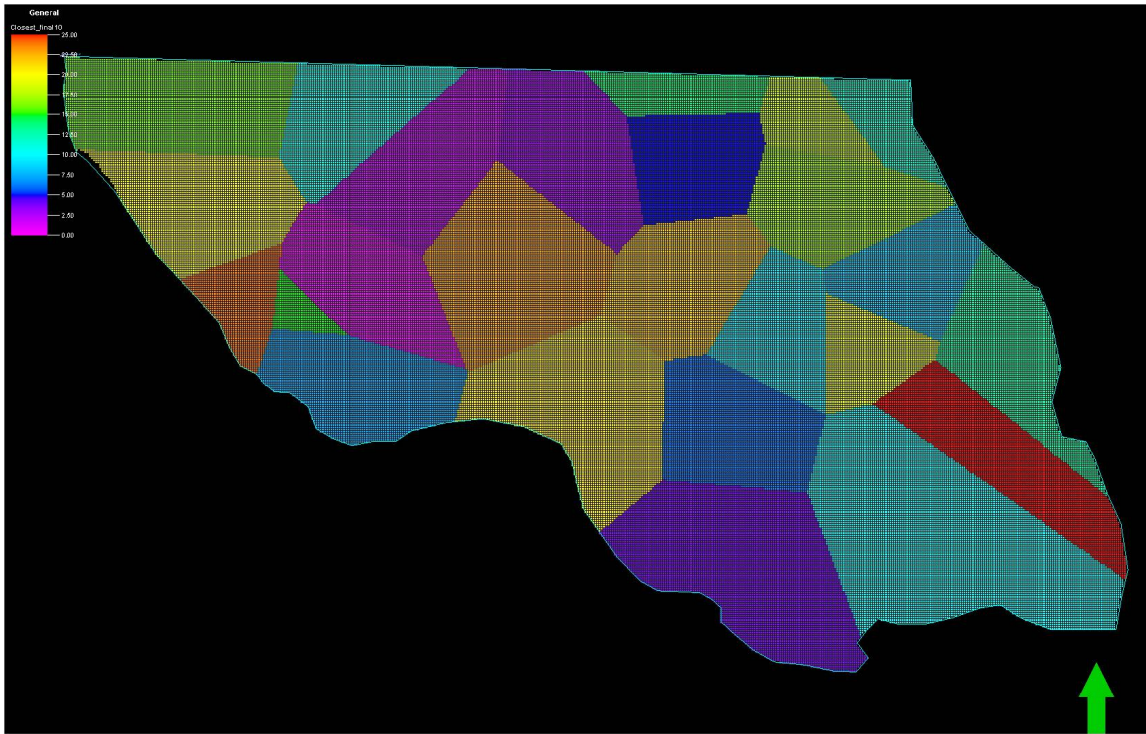
B9. Final areal division (25 subareas) corresponding to 25 pseudo wells in case 10.
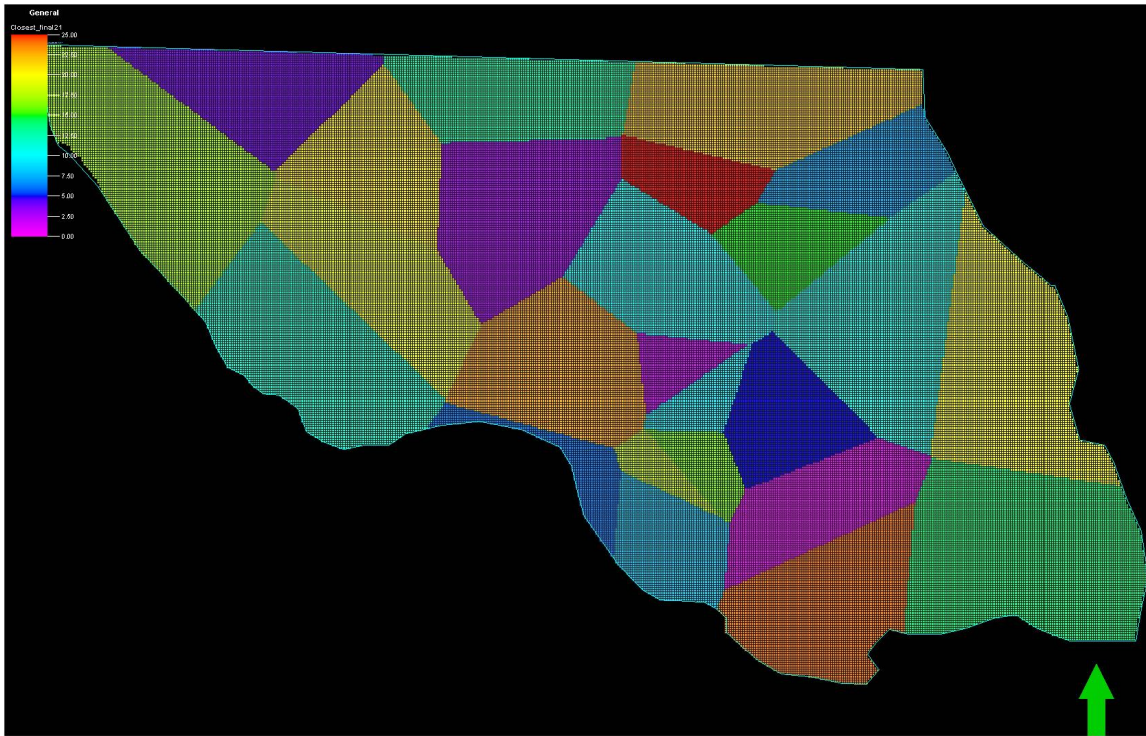
B10. Final areal division (25 subareas) corresponding to 25 pseudo wells in case 11.

B11. Final areal division (25 subareas) corresponding to 25 pseudo wells in case 12.
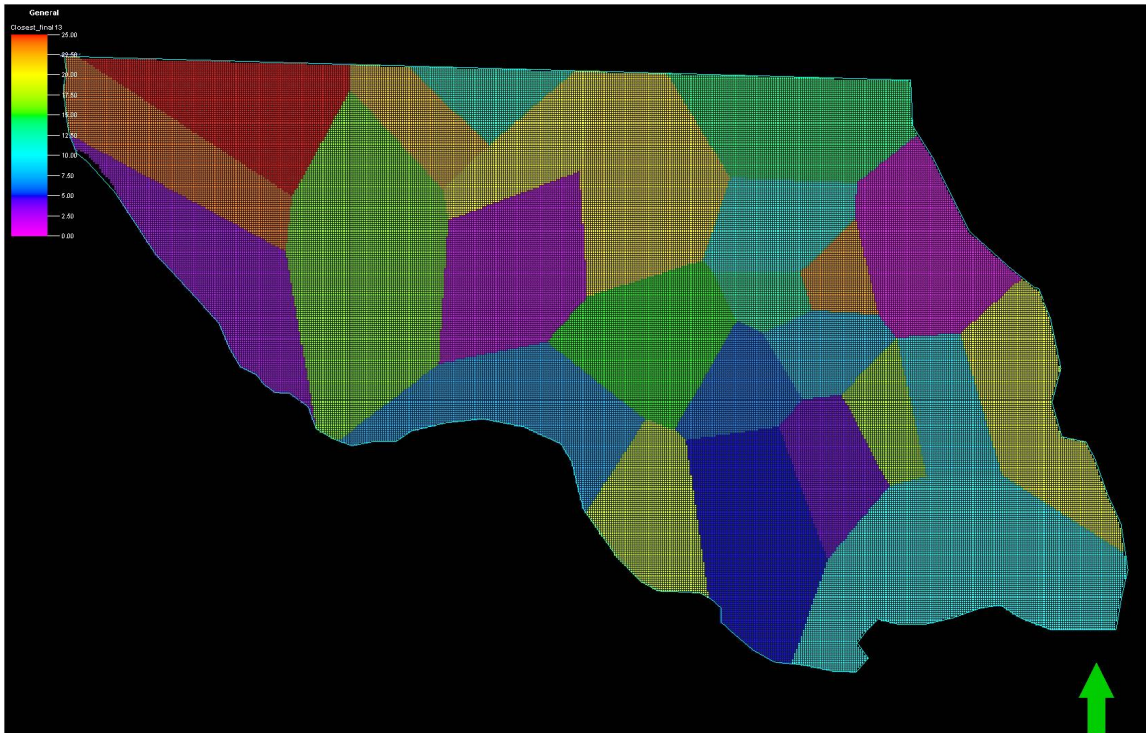
B12. Final areal division (25 subareas) corresponding to 25 pseudo wells in case 13.
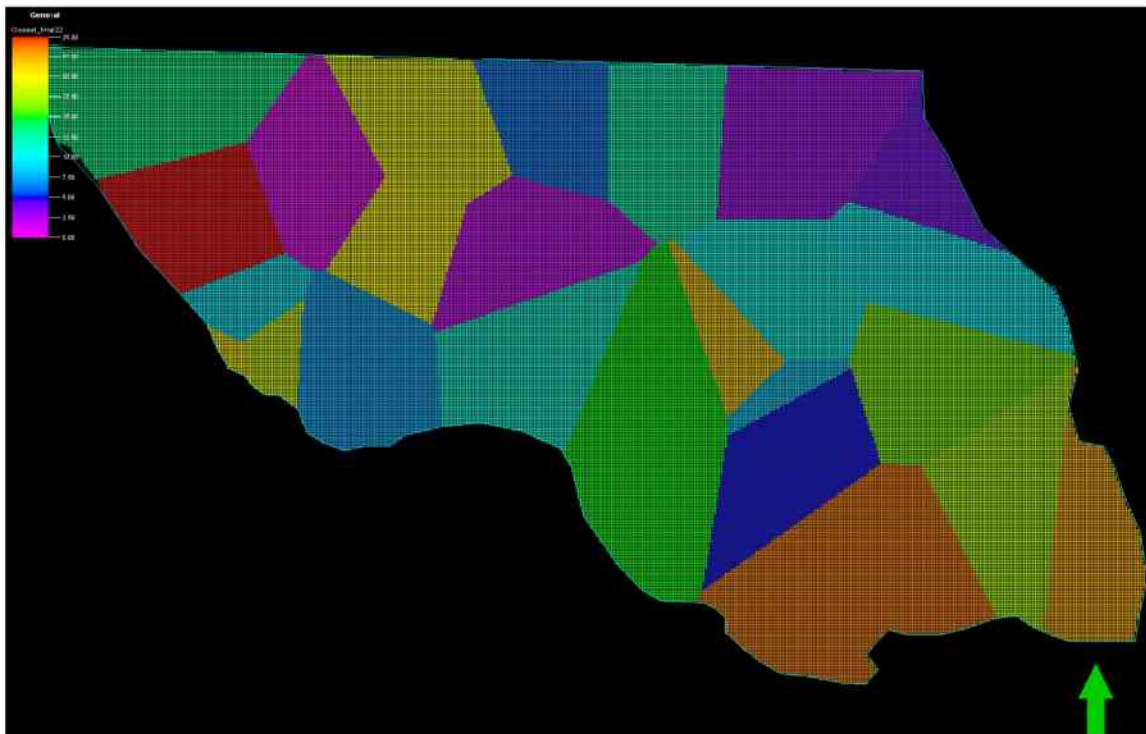
B13. Final areal division (25 subareas) corresponding to 25 pseudo wells in case 14.

B14. Final areal division (25 subareas) corresponding to 25 pseudo wells in case 15.

B15. Final areal division (25 subareas) corresponding to 25 pseudo wells in case 16.

B16. Final areal division (25 subareas) corresponding to 25 pseudo wells in case 17.

B17. Final areal division (25 subareas) corresponding to 25 pseudo wells in case 18.

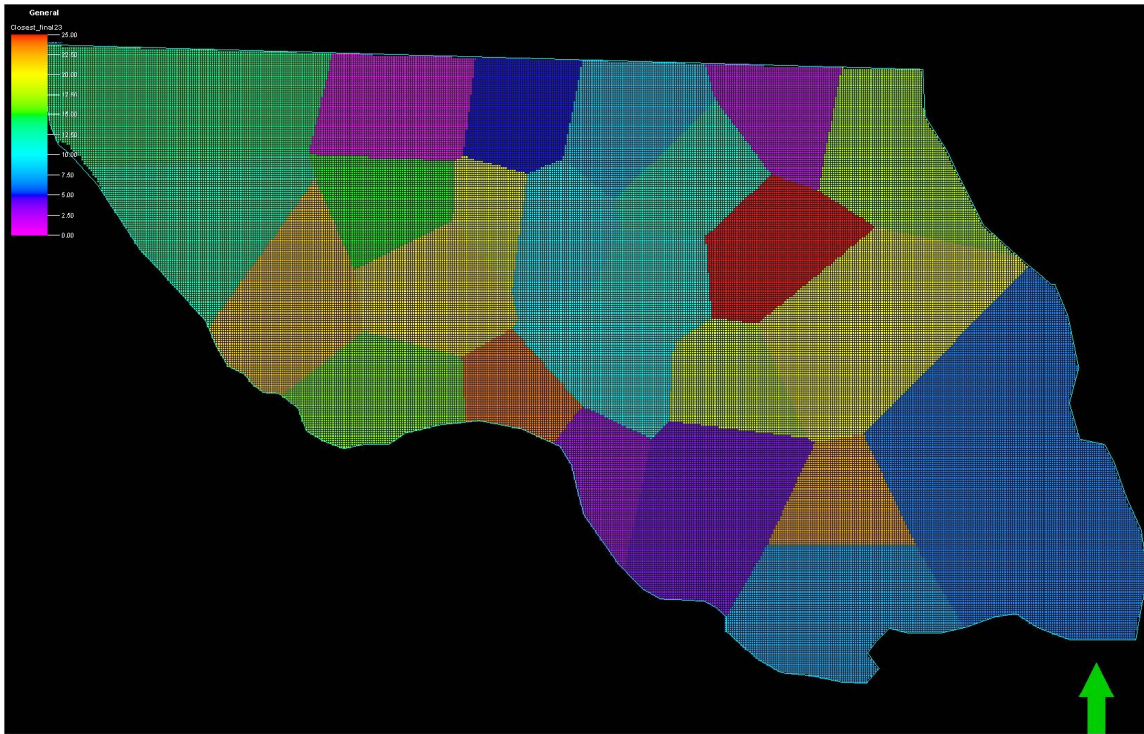B18. Final areal division (25 subareas) corresponding to 25 pseudo wells in case 19.

B19. Final areal division (25 subareas) corresponding to 25 pseudo wells in case 20.
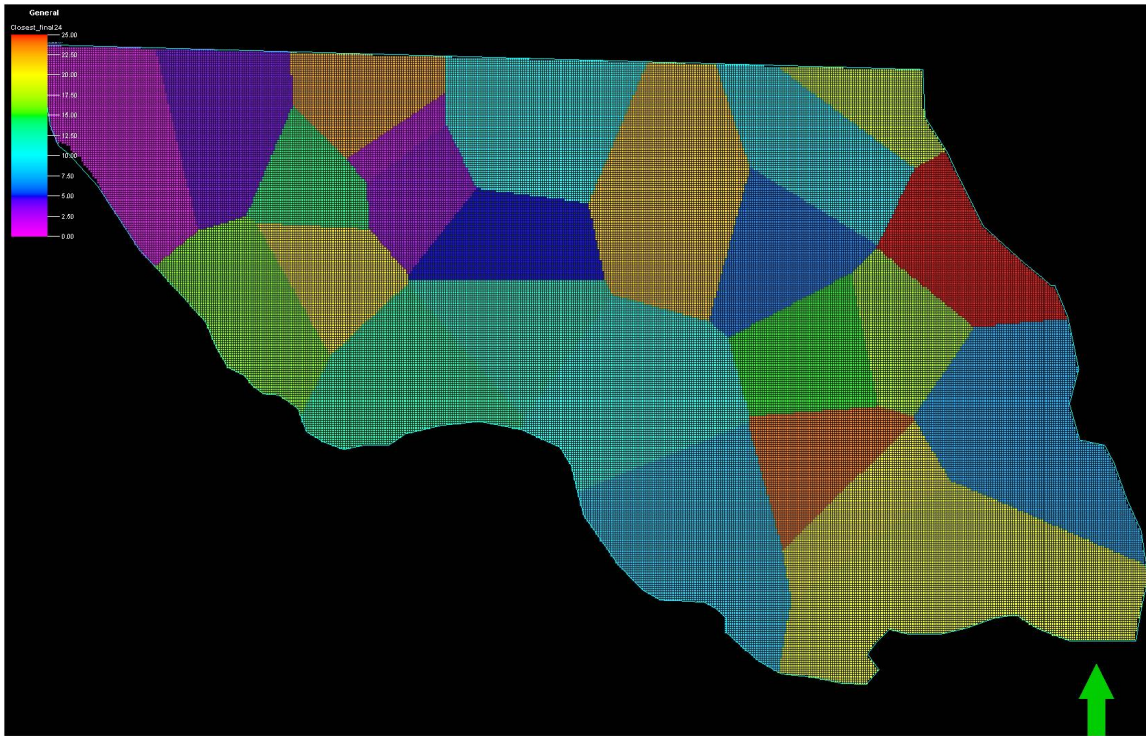
B20. Final areal division (25 subareas) corresponding to 25 pseudo wells in case 21.
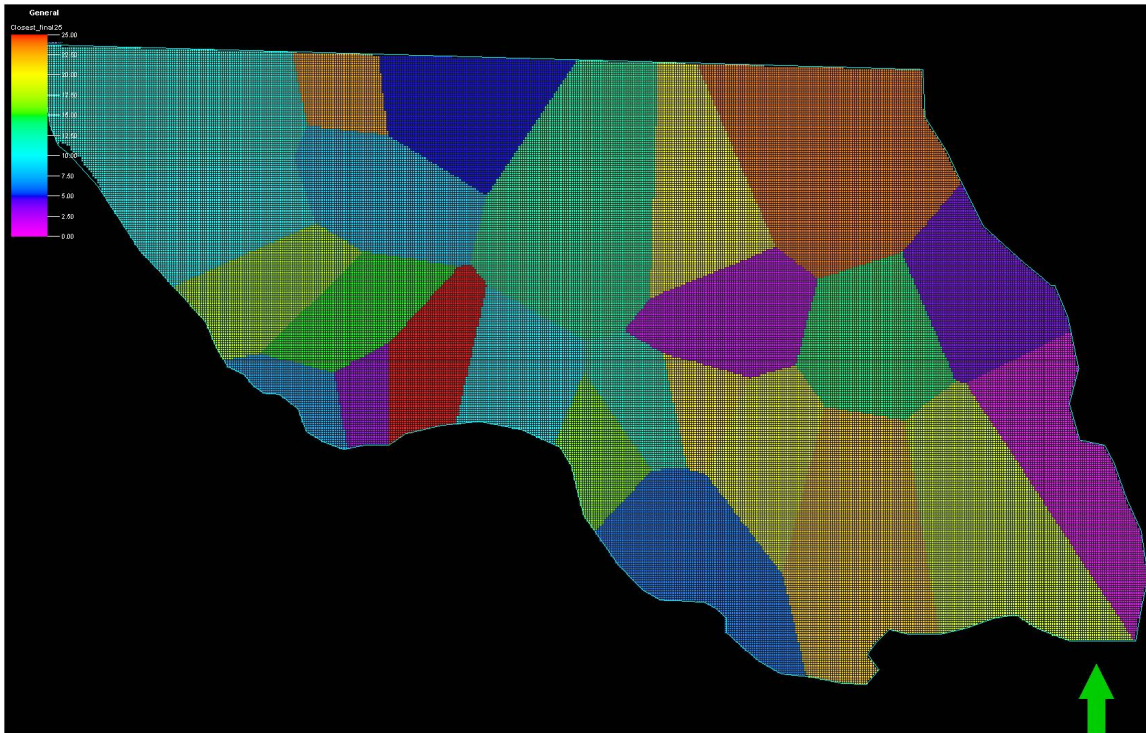
B21. Final areal division (25 subareas) corresponding to 25 pseudo wells in case 22.

B22. Final areal division (25 subareas) corresponding to 25 pseudo wells in case 23.

B23. Final areal division (25 subareas) corresponding to 25 pseudo wells in case 24.

B24. Final areal division (25 subareas) corresponding to 25 pseudo wells in case 25.